observed in cells and tissues from PD patients (Exner et al., 2007; Hoepken et al., 2007). Furthermore, mutations in PD-related genes, such as Parkin, DJ-1, and PINK1, typically present with apparent autosomal recessive inheritance, and affect oxidative stress response pathways and mitochondrial homeostasis (Abeliovich and Flint Beal, 2006). Thus, oxidative stress and disruption of mitochondrial homeostasis have been implicated in the pathogenesis of sporadic and familial PD.

Recent studies have demonstrated that oxidative stress and mitochondrial homeostasis disruption are common mechanisms for motor neuron degeneration in ALS, as well as loss of midbrain dopamine neurons in PD. Mice overexpressing the human A53T mutant α-synuclein (α-syn), a factor for autosomal dominant familial PD, develop severe movement disorder, paralysis, and loss of motor neurons (approximately 75%). In addition, dendritic and axonal inclusions of motor neurons were confirmed by electron microscopy to be due to degenerating mitochondria (Martin et al., 2006). Interestingly, substantianigra (SN) dopaminergic neurons degenerate in a transgenic mouse model of FALS (Andreassen et al., 2001) and in several autopsy cases of human sporadic ALS (Sasaki et al., 1992; Miki et al., 2009). Furthermore, transgenic ALS mice show increased vulnerability to mitochondrial parkinsonian toxins MPTP and 3-nitropropionic acid (Kostic et al., 1997). Pro-apoptotic p53-activated gene 608 (PAG608) has been identified as a specifically induced gene in striatal tissue of L-DOPA-injected hemi-parkinsonian rats. L-DOPA induces PAG608 expression in motor neurons, specifically in the contralateral side of the ventral horn of the spinal cord and the lateral corticospinal tract, without cell loss (Shimizu et al., 2008). Moreover, DJ-1 and PINK1 expression were apparent in spinal motor neurons 8 hr after transient ischemia in a rabbit spinal cord ischemia model (Sakurai et al., 2009).

The present study determined the presence and alterations of PD related-proteins, PINK1, DJ-1, p53, and PAG608, in spinal motor neurons of G93A SOD1 Tg mice, an ALS animal model, to identify whether these proteins are related to ALS pathogenesis.

## MATERIALS AND METHODS

### Animal Model

All experimental procedures were performed according to guidelines published in the NIH *Guide for the Care and Use of Laboratory Animals*, guidelines for the Use of Animals in Neuroscience Research and guidelines from the Animal Care and Use Committee of the Graduate School of Medicine, Dentistry and Pharmaceutical Science of Okayama University. The Tg mice expressing the G93A mutant human SOD1 (strain B6SJL-TGN (G93A SOD1) 1GUR[dl]) were originally obtained from Jackson Laboratory (Bar Harbor, ME; Gurney et al., 1994), and were backcrossed onto a C57BL/6 background strain by mating hemizygote males with inbred C57BL/6 female mice (C57BL/6CrSlc, Nihon SLC, Shizuoka, Japan) to produce Tg and non-Tg wildtype litter-

mate (WT) mice. The G93A SOD1 Tg mice demonstrated disease onset at approximately 15 weeks (15 W), and died at approximately 20 weeks. Three experimental groups were established: 12 W (pre-symptomatic), 17 W (early symptomatic), and 19 W (late symptomatic). Each group comprised five Tg mice and five age-matched WT mice.

### Primary Antibodies

Goat anti-PINK1 (c-20) polyclonal antibody (sc-32584), mouse anti-DJ-1 (D-4) monoclonal antibody (sc-55572), and mouse anti-β-tubulin (D-10) monoclonal antibody (sc-5274) were obtained from Santa Cruz Biotechnology (Santa Cruz, CA). Rabbit anti-phosphorylated p53 (S15) polyclonal antibody (AF1043) was obtained from R&D Systems (Minneapolis, MN). Mouse anti-PAG608 (p53-induced protein) monoclonal antibody (P 2975) was obtained from Sigma-Aldrich (St. Louis, MO).

### Histological Analysis

Animals were deeply anesthetized and transcardially perfused with heparinized saline, followed by 4% paraformaldehyde in 0.1 M phosphate buffer (pH 7.4). The spinal cord region spanning L4–5 was removed and further fixed by immersion in the same fixative for 4 hr. The tissue was then frozen and cryoprotected with a series of phosphate-buffered sucrose solutions of increasing concentration (10, 15, and 20%). Transverse sections, 10 μm thick, were cut through the middle of the L4 segment using a cryostat. Anti-PINK1, DJ-1, and phospho-p53 antibodies were used at a dilution of 1:100 after blocking sections in 5% bovine serum albumin. Anti-PAG608 antibody was used at a dilution of 1:100 after blocking sections in TNB blocking buffer (PerkinElmer, Waltham MA). The incubations were performed overnight at 4°C. Immunohistochemical analysis was performed using standard fluorescence methods or peroxidase labeling with the Vectastain avidin:biotinylated enzyme complex (ABC) kit (Vector Laboratories, Youngstown, OH). For double staining of phospho-p53/PAG608, sections were incubated with rabbit anti-phospho-p53 polyclonal antibody (1:100) and mouse anti-PAG608 monoclonal antibody (1:100) at 4°C overnight, washed three times with PBS, then were hybridized and visualized with rhodamine-conjugated anti-rabbit IgG secondary antibody (1:400; Chemicon, Temecula, CA) and FITC-conjugated anti-mouse IgG secondary antibody (1:400; Chemicon), respectively. Relevant negative controls were stained without primary antibodies in parallel.

### Motor Neuron Quantification

To evaluate the percentage of immunopositive motor neurons, preserved motor neurons in the L4 segment were quantified in five transverse sections from each lumbar cord following cresyl violet staining (Nissl stain). All cells in the ventral horns, below a lateral line across the spinal cord from the central canal, were microscopically video-captured, and only cells with a diameter greater than 20 μm with a clear nucleoli were quantified by investigators, who were blinded to the sample information, as described previously (Ohta et al., 2006). An average of five sections was used to represent

the number of living motor neurons in each animal. In addition, each mouse section was immunostained with anti-choline acetyltransferase antibody (ChAT goat antiserum; Chemicon) to confirm quantification results of motor neurons.

### Western Blot Analysis

Western blot analysis was performed using the ventral portion of lumbar spinal cords from five mice of each group. A total of 0.3 mL cold lysis buffer (50 mM Tris-HCl, pH 7.2, 10% glycerol, 250 mM NaCl, 0.1% NP-40, 2 mM EDTA, and protease inhibitors) was added to the spinal cord tissue, and the tissue was sonicated on ice. The sonicates were centrifuged at 12,000$g$ for 10 min at 4°C, and the supernatants were collected for Western blot analysis, which was performed using standard techniques and an ECL Plus detection kit (GE Healthcare, Cleveland, OH). Blot images were captured and quantified using a luminoimage analyzer (LAS 1000-mini, Fuji Film, Tokyo, Japan).

The anti-PINK1, DJ-1, and PAG608 antibodies were used at a dilution of 1:500, and anti β-tubulin antibody at a dilution of 1:1000. The HRP-conjugated anti-goat IgG secondary antibody (Amersham Biosciences, Buckinghamshire, UK) and HRP-conjugated anti-mouse IgG secondary antibody (Amersham Biosciences) were used at a dilution of 1:2000. Densitometry analysis was performed with Scion Image Beta 4.02 software using an average value from five mice.

### Statistical Analysis

Quantitative analyses of the number of motor neuron and optical density of Western blot results were analyzed by ANOVA. A $P$-value $< 0.05$ was considered to be statistically significant. Parametric data were presented as mean $\pm$ SD.

## RESULTS

### Expression of PINK1 and DJ-1 Increased in the Spinal Cord of Tg Mice

To investigate changes in PINK1 and DJ-1 expression during the progression of ALS symptoms, immunohistochemical analysis and immunoblotting were performed on lumbar spinal cord sections from WT and Tg mice at 12 W (pre-symptomatic stage), 17 W (early symptomatic stage), and 19 W (late symptomatic stage). In the Tg mice, Nissl staining revealed progressively decreased numbers of motor neurons with age (Fig. 1A, top), and immunohistochemical staining demonstrated increased PINK1 immunoreactivity with age (Fig. 1A, middle). At 19 W, DJ-1 immunoreactivity also increased, and exhibited a nuclear staining (Fig. 1A, bottom). PINK1 and DJ-1 seem to be localized in small cells as well as motor neurons of Tg mice at 17 W and 19 W (Fig. 1A, middle and bottom).

Extracts of lumbar spinal cords were used to quantify protein expressions of PINK1 and DJ-1 on Western blot. PINK1 protein expression (relative to β-tubulin) was greater in 17 W-aged Tg mice [0.30 $\pm$ 0.11 (WT) vs. 0.77 $\pm$ 0.32 (Tg) (*$P < 0.05$, n = 5)] and in 19 W-aged Tg mice [0.30 $\pm$ 0.11 (WT) vs. 0.87 $\pm$ 0.36 (Tg) (*$P < 0.05$, n = 5)] than in WT mice. However, there
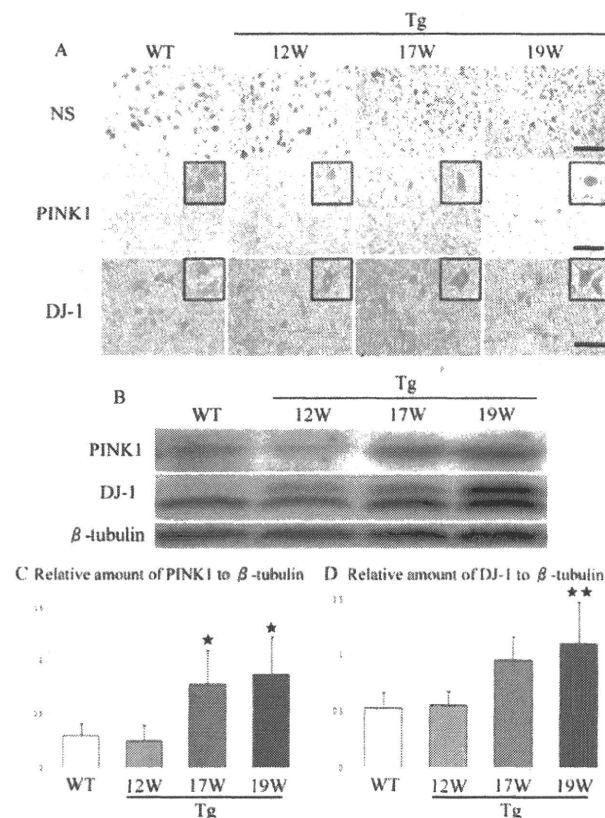


Fig. 1. Increased expression of PINK1 and DJ-1 in the spinal cord of Tg mice. **A:** Immunohistochemical analysis of PINK1 and DJ-1 in the lumbar spinal cords of WT and Tg mice. Note that while Nissl staining (NS) showed that the number of living motor neurons decreased in Tg mice at 17 W and 19 W of age (top), PINK1 staining was remarkably increased with age in Tg mice (middle). DJ-1 nuclear staining increased in Tg mice at 19 W (bottom). PINK1 and DJ-1 seem to be localized in small cells as well as motor neurons of Tg mice at 17 W and 19 W. Scale bars = 100 μm **(B)** Western blot analysis of PINK1 and DJ-1 in the lumbar spinal cords of WT and Tg mice. (B,C) The amounts of PINK1 (relative to β-tubulin) were greater in 17 W Tg mice (*$P < 0.05$, n = 5) and in 19 W Tg mice, compared with WT mice (*$P < 0.05$, n = 5) (B,D). DJ-1 levels (relative to β-tubulin) were greater in 17 W Tg mice, and differences to WT became significant at 19 W (**$P < 0.01$, n = 5). [Color figure can be viewed in the online issue, which is available at www.interscience.wiley.com.]

was no significant difference between WT mice and 12 W-aged Tg mice [0.30 $\pm$ 0.11 (WT) vs. 0.25 $\pm$ 0.14 (Tg) (n = 5) (Fig. 1B,C)]. In addition, DJ-1 protein expression (relative to β-tubulin) was greater in 19 W-aged Tg mice compared with WT mice [0.53 $\pm$ 0.14 (WT) vs. 1.10 $\pm$ 0.38 (Tg) (**$P < 0.01$, n = 5)], but there was no significant difference between WT mice and 12 W-aged Tg mice [0.53 $\pm$ 0.14 (WT) vs. 0.54 $\pm$ 0.13 (Tg) (n = 5)], and between WT mice and 17 W-aged Tg mice [0.53 $\pm$ 0.14 (WT) vs. 0.94 $\pm$ 0.22 (Tg) (n = 5)] (Fig. 1B,D).
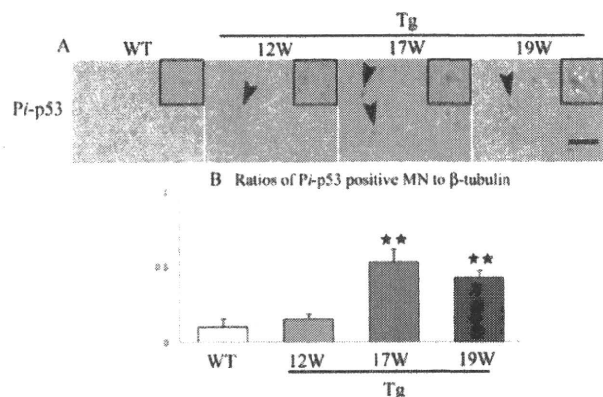
Fig. 2. Increased levels of phosphorylated p53 in motor neuron nuclei in the spinal cords of Tg mice. **A:** Immunohistochemical analysis of phosphorylated p53 (P$i$-p53) in the lumbar spinal cords of WT and Tg mice. Note that the motor neurons of the lumbar spinal cord in Tg mice exhibited more intense P$i$-p53 expression at 17 W and 19 W, compared with WT mice, and cytoplasmic staining was stronger with age in Tg mice, with accumulated nuclear expression (arrowheads). Scale bar = 100 μm (**B**) The ratios of immunopositive motor neurons to mean total living motor neurons of each Tg mice and WT mice, revealing the average ratios of P$i$-p53 were significantly greater in 17 W Tg mice (**$P < 0.01$, n = 5) and 19 W Tg mice (**$P < 0.01$, n = 5), compared with WT mice. [Color figure can be viewed in the online issue, which is available at www.interscience.wiley.com.]

### Increased Phosphorylated p53 in Motor Neuron Nuclei in the Spinal Cords of Tg Mice

To investigate the presence and altered expression of p53 in motor neurons of the ALS model mouse, immunohistochemical analysis was performed in the lumbar spinal cords of WT and Tg mice. There was no significant difference in total p53 immunoreactivity in the lumbar spinal cords of WT mice and Tg mice (data not shown). In contrast, motor neurons of from lumbar spinal cord in Tg mice exhibited more intense immunopositive staining for serine 15-phosphorylated p53 (P$i$-p53), an activated form of p53, at 17 W and 19 W, compared with WT mice (Fig. 2A). Although P$i$-p53 immunoreactivity was more intense in 12 W-aged Tg mice compared with WT mice, the difference was not significant. P$i$-p53 immunostaining was weak and diffuse in spinal motor neurons of WT mice, while cytoplasmic staining was stronger with age in the Tg mice, with increasing nuclear expression (Fig. 2A arrowheads). When ratios of immunopositive motor neurons to mean total motor neurons were calculated, the average P$i$-p53 ratios were significantly greater in the 17 W-aged Tg mice [(0.10 ± 0.06 (WT) vs. 0.52 ± 0.09 (Tg) (**$P < 0.01$, n = 5)] and in the 19 W-aged Tg mice [0.10 ± 0.06 (WT) vs. 0.42 ± 0.05 (Tg) (**$P < 0.01$, n = 5)] compared with the WT mice (Fig. 2B).

### Increased PAG608 Expression in the Spinal Cord of Tg Mice

Expression of PAG608, a p53 activated protein that is co-activated with p53 to promote apoptosis, was meas-
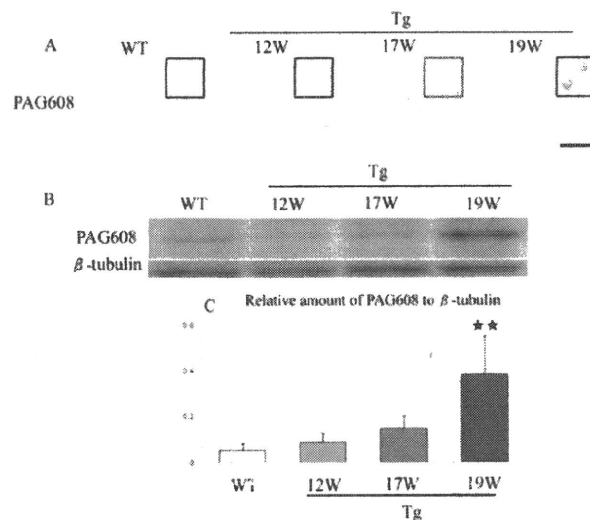
Fig. 3. Increased PAG608 expression in the spinal cord of Tg mice. **A:** Immunohistochemical analysis of PAG608, a protein p53 activated by p53, in the motor neurons of WT and Tg mice. Note that PAG608 expression was hardly observed in WT and 12 W Tg mice, but there was intense cytoplasmic and nuclear PAG608 expression in 17 W and 19 W Tg mice. Scale bar = 100 μm (**B,C**) Western blot analysis of PAG608 from lumbar spinal cord extracts of WT and Tg mice revealed significantly greater PAG608 expression (relative to β-tubulin) in 19 W Tg mice, compared with WT mice (**$P < 0.01$, n = 5). [Color figure can be viewed in the online issue, which is available at www.interscience.wiley.com.]

ured in lumbar spinal cord motor neurons of ALS and WT mice using immunohistochemical analysis. PAG608 immunoreactivity was very weak in the lumbar spinal cords of WT mice and 12 W-aged Tg mice. In contrast, intense PAG608 expression was observed in the lumbar spinal cords of 17 W- and 19 W-aged Tg mice (Fig. 3A). In particular, markedly condensed PAG608-positive signals were observed in the nucleolus of 19 W-aged Tg mice.

PAG608 Western blot analysis was performed on extracts of lumbar spinal cords. Protein levels of PAG608 (relative to β-tubulin) were greater in 19 W-aged Tg mice (0.381 ± 0.17) than in WT mice (0.052 ± 0.03; **$P < 0.01$, n = 5). However, there was no significant difference between WT (0.052 ± 0.03) and 12 W-aged Tg (0.086 ± 0.04) or 17 W-aged Tg (0.146 ± 0.06) (Fig. 3B,C).

### PAG608 and P$i$-p53 Proteins are Co-expressed in Spinal Neurons of Tg Mice

Immunofluorescence analysis of P$i$-p53 and PAG608 were performed in anterior spinal cord sections of WT mice and 19 W aged Tg mice. P$i$-p53 was strongly expressed in the nuclei of spinal motor neurons in Tg mice, but not in WT mice (Fig. 4, top). PAG608 was also strongly expressed in the nuclei and cytoplasm of Tg spinal motor neurons, but was only weakly expressed in the cytoplasm of WT spinal neurons
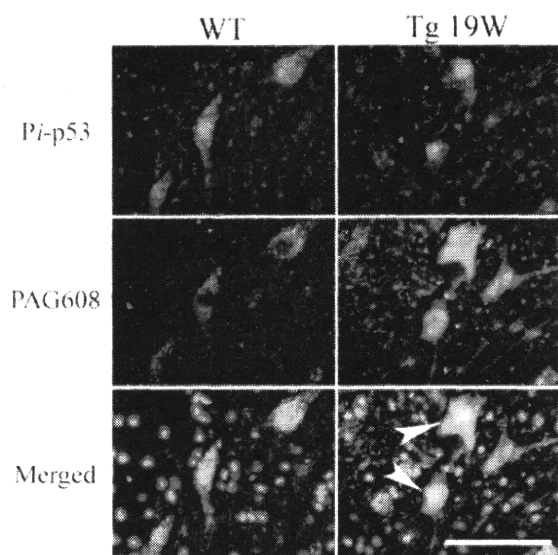
WT          Tg 19W



Pi-p53

PAG608

Merged

Fig. 4. PAG608 and Pi-p53 are co-expressed in the spinal neurons of Tg mice. Immunofluorescence analysis of Pi-p53 and PAG608 in anterior spinal cord sections of WT mice and 19 W Tg mice, showing strong nuclear expression of Pi-53 in spinal motor neurons of Tg mice, but not in WT mice (top), as well as strong nuclear and cytoplasmic expression of PAG608 (middle). Note co-expression of Pi-p53 and PAG608 in nuclei of spinal neurons in 19 W Tg mice (bottom, arrowheads). Scale bar = 100 μm. [Color figure can be viewed in the online issue, which is available at www.interscience.wiley.com.]

(Fig. 4, middle). Moreover, PAG608 was co-expressed with Pi-p53 in the nuclei of spinal neurons from 19 W-aged Tg mice (Fig. 4, bottom).

## DISCUSSION

The present study investigated the presence and alterations of Parkinson's disease-related proteins in spinal motor neurons of G93ASOD1 Tg mice, an ALS animal model. Results demonstrated increased PINK1 and DJ-1 protein expression in the Tg mice following disease onset (Fig. 1). p53 became activated and translocated to the nuclei of spinal motor neurons, which, in turn, activated the specific expression of PAG608 (Figs. 2–3). This is the first report demonstrating that PAG608 and Pi-p53 protein levels are increased and co-expressed in an ALS model animal (Fig. 4).

The PINK1 gene encodes a ubiquitously expressed, insoluble, 581-amino acid, 63-kDa protein, with an 8-kDa amino-terminal, mitochondrial-targeting sequence. The complete protein is transcribed in the nucleus, translated in the cytoplasm, and imported intact into mitochondria, with subsequent processing and intramitochondrial sorting. There is some evidence that PINK1 is localized in the inner mitochondrial membrane (Schapira, 2008). Mutations in PINK1 result in autosomal recessive PD (Valente et al., 2004). A recent study reported that PINK1 protein is increased in the brains of PD patients (Muqit et al., 2006), indicating that PINK1

may be up-regulated in response to PD-related stress. Moreover, PINK1 is selectively increased in spinal motor neuron cells following transient spinal cord ischemia in rabbits (Sakurai et al., 2009), suggesting that oxidative stress induces PINK1 expression as a compensatory mechanism. The present study demonstrated that PINK1 expression increased in the spinal cords of Tg mice at early and late symptomatic stages (Fig. 1). These results suggested that PINK1 is up-regulated in response to mitochondrial oxidative damage, which has been previously reported in spinal motor neurons of ALS model mice (Warita et al., 2001; Murakami et al., 2007).

The DJ-1 gene encodes a small 189 amino acid protein that is ubiquitously expressed and highly conserved in diverse species (Bai et al., 2006). The DJ-1 protein is multi-functional and plays roles in transcriptional regulation and anti-oxidative stress functions, and loss of its functions leads to onset of PD and cancer (Nagakubo et al., 1997). Although DJ-1 does not directly bind to DNA, DJ-1 acts as a co-activator of various transcription factors, including the androgen receptor and p53. DJ-1 is also known as an anti-oxidative stress factor, and its function is achieved through various mechanisms. DJ-1 is self-oxidized at cysteine residues at amino acids 46, 53, and 106 (C46, C53, and C106, respectively), resulting in elimination of reactive oxygen species. DJ-1 transactivates genes whose products contribute to the redox reaction, including glutathione synthetase and SOD3. In addition, DJ-1 facilitates nuclear translocation of Nrf2, a master transcription factor for anti-oxidation-related genes, by sequestering Keap1, a negative regulator of Nrf2. Absence of the reduced form of DJ-1, and the presence of abnormally oxidized DJ-1, has been observed in PD patient brains, and the accumulation of highly oxidized DJ-1 has been measured in patients with PD and Alzheimer's disease (Tsuboi et al., 2008). It is of particular interest that DJ-1 protects against neurodegeneration due to focal cerebral ischemia in rats (Yanagisawa et al., 2008).

In the present study, DJ-1 expression increased in the spinal cord of Tg mice during late symptomatic stages (Fig. 1). These results suggested that DJ-1 up-regulates in response to oxidative stress in motor neurons in ALS model mice. However, immunohistological results demonstrated that it is regardless if increased DJ-1 is highly oxidized or not, because anti-total DJ-1 antibody was utilized. Studies have reported increased DJ-1 mRNA and protein levels in brains and spinal cords of G93A SOD1 Tg mice, compared with WT controls (Lev et al., 2009), showing that increased DJ-1 acidic isoforms could be detected. Therefore, more oxidized forms of DJ-1 mostly likely exist in the CNS of SOD1G93A mice.

Previous reports suggested that glial cells may promote neuronal survival by providing trophic, metabolic and antioxidant support, and not only stimulate apoptosis via diffusible factors that activate death receptors in ALS (Barbeito et al., 2004; Vargas et al., 2006). In our immunohistochemical analysis, PINK1 and DJ-1 do not seem

to be localized only in motor neurons but also in small cells. Although PINK1 and DJ-1 localization and expression in small cells need to be further investigated, they may be related to the non cell autonomous effect between motor neurons and glial cells which has lately attracted considerable attention.

p53 acts as a pro-apoptotic transcriptional factor (Prives and Hall, 1999), and a recent study reported that p53 phosphorylation at serine 15 enhances its transactivation capacity (Shieh et al., 1997). Moreover, increased Pi-p53 was demonstrated in the substantia nigra pars compacta of post-mortem PD brains (de la Monte et al., 1998). Moreover, increased levels of phosphorylated p53 were detected prior to the emergence of apoptotic features in an in vitro study of PD. Proteasome-inhibited cells, however, did not express increased p53 mRNA, suggesting that p53 is activated in a transcription-independent manner (Nair et al., 2006). In the study, there was no significant difference between immunoreactivity of total p53 in lumbar spinal cords of WT mice and Tg mice (data not shown). In contrast, serine 15-phosphorylated p53 (Pi-p53) was increased in the motor neurons of the lumbar spinal cord of Tg mice at 17 W and 19 W (Fig. 2A), which was consistent with increased Pi-p53 following G86R mutant SOD1 expression (Gonzalez de Aguilar et al., 2000). These findings were similar to altered p53 expression observed in PD patients and animal models (de la Monte et al., 1998; Nair et al., 2006; Duke et al., 2007; Mogi et al., 2007). These studies suggest that p53 activation in G93ASOD1 Tg mice is partly controlled in a transcription-independent manner. Nevertheless, wobbler mice, which exhibit rapid motor neuronal cell death, as well as human ventral horns obtained from ALS patients, demonstrate increased p53 gene expression (Eve et al., 2007). Therefore, transcriptional up-regulation and activation through protein phosphorylation may play a role together in motor neuron death in ALS.

p53 has been reported to translocate to nuclei of spinal cord neurons in G86RSOD1 transgenic mice (Gonzalez de Aguilar et al., 2000), and nuclear localization has previously been shown to correlate with p53 activation (Shaulsky et al., 1991). The present study demonstrated accumulation of p53 in the nuclei of motor neurons in G93ASOD1 Tg mice (Fig. 2A). This suggested that p53 signaling pathway is activated through phosphorylation of serine 15 and nuclear translocation in G93ASOD1 Tg mice. Moreover, DJ-1 exerts cytoprotective effects by inhibiting the p53-Bax-caspase pathway, as well as interacting with p53 in vitro and in vivo (Fan et al., 2008). Therefore, increased DJ-1 (also shown in Fig. 1) may have a cytoprotective role by protecting from oxidative stress, as well as inhibiting the p53 pathway in G93ASOD1 Tg mice.

PAG608 is a pro-apoptotic gene, which is activated by p53 induction and thereby promotes apoptosis. It is abundantly expressed in the central nervous system (Varmeh-Ziaie et al., 1997), with increased expression reported in the hippocampus following transient cerebral

ischemia, accompanied by accumulation of p53, caspase-3, and phospho-c-Jun (Gillardon et al., 1999; Tomasevic et al., 1999; Hermann et al., 2001). Previous studies suggested a pro-apoptotic role for PAG608 in oxidative stress-induced catecholaminergic cell death. Following treatment with the dopaminergic neurotoxin 6-OHDA, PAG608 results in inverse induction of p53 and Bax, as well as reduced mitochondrial membrane potential during apoptotic changes in catecholaminergic PC12 cells (Higashi et al., 2002). In addition, PAG608 has been identified as a specifically induced gene in striatal tissue of L-DOPA (100 mg/kg)-injected hemi-parkinsonian rats using differential display assay. It is of great interest that L-DOPA has been shown to induce PAG608 expression in motor neurons, specifically in the contralateral side of the ventral horn of the spinal cord and the lateral corticospinal tract, without cell loss in the hemi-parkinsonian rats (Shimizu et al., 2008). When dopaminergic neurons are damaged in Parkinsonian models, excess L-DOPA administration produces dopamine quinines, which exert pathogenic effects of dopaminergic neuron-specific oxidative stress in the striatum (Asanuma et al., 2003; Miyazaki and Asanuma, 2009). Therefore, excess dopamine, as a result of L-DOPA administration, differentially stimulates the extrapyramidal tract connecting to the pyramidal tract and lower spinal motor neurons, and may activate or stress lower spinal motor neurons. These data suggest that PAG608 may be a useful marker for stressed or activated lower motor neurons. In the present study, increased PAG608 expression was observed in G93A SOD1 Tg mice during late symptomatic stages (Fig. 3), and it co-expressed with Pi-p53 in the nuclei of spinal neurons (Fig. 4). These results suggested that spinal motor neurons of G93ASOD1 Tg mice were exposed to the p53-related cell death signaling pathway as a result of stress. Although further studies are needed to clarify the role of PAG608 in motor neurons and its nucleolar localization, PAG608 may be a useful marker for identifying stressed motor neurons in ALS.

Also, our present study provides further evidence of the profound correlation between parkinsonism-related proteins and ALS pathology. These results are important to investigate the potential common therapeutic targets of PD and ALS.

## REFERENCES

Abe K, Pan LH, Watanabe M, Kato T, Itoyama Y. 1995. Induction of nitrotyrosine-like immunoreactivity in the lower motor neuron of amyotrophic lateral sclerosis. Neurosci Lett 199:152–154.

Abeliovich A, Flint Beal M. 2006. Parkinsonism genes: culprits and clues. J Neurochem 99:1062–1072.

Andreassen OA, Ferrante RJ, Klivenyi P, Klein AM, Dedeoglu A, Albers DS, Kowall NW, Beal MF. 2001. Transgenic ALS mice show increased vulnerability to the mitochondrial toxins MPTP and 3-nitropropionic acid. Exp Neurol 168:356–363.

Aoki M, Ogasawara M, Matsubara Y, Narisawa K, Nakamura S, Itoyama Y, Abe K. 1993. Mild ALS in Japan associated with novel SOD mutation. Nat Genet 5:323–324.

Asanuma M, Miyazaki I, Ogawa N. 2003. Dopamine- or L-DOPA-induced neurotoxicity: the role of dopamine quinone formation and tyrosinase in a model of Parkinson's disease. Neurotox Res 5:165–176.

Bai Q, Mullett SJ, Garver JA, Hinkle DA, Burton EA. 2006. Zebrafish DJ-1 is evolutionarily conserved and expressed in dopaminergic neurons. Brain Res 1113:33–44.

Barbeito LH, Pehar M, Cassina P, Vargas MR, Peluffo H, Viera L, Estevez AG, Beckman JS. 2004. A role for astrocytes in motor neuron loss in amyotrophic lateral sclerosis. Brain Res Brain Res Rev 47:263–274.

Bendotti C, Calvaresi N, Chiveri L, Prelle A, Moggio M, Braga M, Silani V, De Biasi S. 2001. Early vacuolization and mitochondrial damage in motor neurons of FALS mice are not associated with apoptosis or with changes in cytochrome oxidase histochemical reactivity. J Neurol Sci 191:25–33.

Bove J, Prou D, Perier C, Przedborski S. 2005. Toxin-induced models of Parkinson's disease. NeuroRx 2:484–494.

Bowling AC, Barkowski EE, McKenna-Yasek D, Sapp P, Horvitz HR, Beal MF, Brown RH Jr. 1995. Superoxide dismutase concentration and activity in familial amyotrophic lateral sclerosis. J Neurochem 64:2366–2369.

de la Monte SM, Sohn YK, Ganju N, Wands JR. 1998. P53- and CD95-associated apoptosis in neurodegenerative diseases. Lab Invest 78:401–411.

Duke DC, Moran LB, Pearce RK, Graeber MB. 2007. The medial and lateral substantia nigra in Parkinson's disease: mRNA profiles associated with higher brain tissue vulnerability. Neurogenetics 8:83–94.

Eve DJ, Dennis JS, Citron BA. 2007. Transcription factor p53 in degenerating spinal cords. Brain Res 1150:174–181.

Exner N, Treske B, Paquet D, Holmstrom K, Schiesling C, Gispert S, Carballo-Carbajal I, Berg D, Hoepken HH, Gasser T, Kruger R, Winklhofer KF, Vogel F, Reichert AS, Auburger G, Kahle PJ, Schmid B, Haass C. 2007. Loss-of-function of human PINK1 results in mitochondrial pathology and can be rescued by parkin. J Neurosci 27:12413–12418.

Fan J, Ren H, Jia N, Fei E, Zhou T, Jiang P, Wu M, Wang G. 2008. DJ-1 decreases Bax expression through repressing p53 transcriptional activity. J Biol Chem 283:4022–4030.

Gillardon F, Spranger M, Tiesler C, Hossmann KA. 1999. Expression of cell death-associated phospho-c-Jun and p53-activated gene 608 in hippocampal CA1 neurons following global ischemia. Brain Res Mol Brain Res 73:138–143.

Gonzalez de Aguilar JL, Gordon JW, Rene F, de Tapia M, Lutz-Bucher B, Gaiddon C, Loeffler JP. 2000. Alteration of the Bcl-x/Bax ratio in a transgenic mouse model of amyotrophic lateral sclerosis: evidence for the implication of the p53 signaling pathway. Neurobiol Dis 7:406–415.

Gurney ME, Pu H, Chiu AY, Dal Canto MC, Polchow CY, Alexander DD, Caliendo J, Hentati A, Kwon YW, Deng HX 1994. Motor neuron degeneration in mice that express a human Cu,Zn superoxide dismutase mutation. Science 264:1772–1775.

Hermann DM, Kuroiwa T, Hata R, Gillardon F, Ito U, Mies G. 2001. Expression of redox factor-1, p53-activated gene 608 and caspase-3 messenger RNAs following repeated unilateral common carotid artery occlusion in gerbils—relationship to delayed cell injury and secondary failure of energy state. Neuroscience 102:779–787.

Higashi Y, Asanuma M, Miyazaki I, Haque ME, Fujita N, Tanaka K, Ogawa N. 2002. The p53-activated gene, PAG608, requires a zinc finger domain for nuclear localization and oxidative stress-induced apoptosis. J Biol Chem 277:42224–42232.

Hoepken HH, Gispert S, Morales B, Wingerter O, Del Turco D, Mulsch A, Nussbaum RL, Muller K, Drose S, Brandt U, Deller T, Wirth B, Kudin AP, Kunz WS, Auburger G. 2007. Mitochondrial dysfunction, peroxidation damage and changes in glutathione metabolism in PARK6. Neurobiol Dis 25:401–411.

Kostic V, Gurney ME, Deng HX, Siddique T, Epstein CJ, Przedborski S. 1997. Midbrain dopaminergic neuronal degeneration in a transgenic mouse model of familial amyotrophic lateral sclerosis. Ann Neurol 41:497–504.

Lev N, Ickowicz D, Barhum Y, Melamed E, Offen D. 2009. DJ-1 changes in G93A-SOD1 transgenic mice: implications for oxidative stress in ALS. J Mol Neurosci 38:94–102.

Martin LJ, Pan Y, Price AC, Sterling W, Copeland NG, Jenkins NA, Price DL, Lee MK. 2006. Parkinson's disease alpha-synuclein transgenic mice develop neuronal mitochondrial degeneration and cell death. J Neurosci 26:41–50.

Miki Y, Mori F, Nunomura J, Ookawa K, Yajima N, Yagihashi S, Wakabayashi K. 2009. Sporadic amyotrophic lateral sclerosis with pallido-nigro-luysian degeneration: a TDP-43 immunohistochemical study. Neuropathology (In Press).

Miyazaki I, Asanuma M. 2009. Approaches to prevent dopamine quinone-induced neurotoxicity. Neurochem Res 34:698–706.

Mogi M, Kondo T, Mizuno Y, Nagatsu T. 2007. p53 protein, interferon-gamma, and NF-kappaB levels are elevated in the parkinsonian brain. Neurosci Lett 414:94–97.

Muqit MM, Abou-Sleiman PM, Saurin AT, Harvey K, Gandhi S, Deas E, Eaton S, Payne Smith MD, Venner K, Matilla A, Healy DG, Gilks WP, Lees AJ, Holton J, Revesz T, Parker PJ, Harvey RJ, Wood NW, Latchman DS. 2006. Altered cleavage and localization of PINK1 to aggresomes in the presence of proteasomal stress. J Neurochem 98:156–169.

Murakami T, Nagai M, Miyazaki K, Morimoto N, Ohta Y, Kurata T, Takehisa Y, Kamiya T, Abe K. 2007. Early decrease of mitochondrial DNA repair enzymes in spinal motor neurons of presymptomatic transgenic mice carrying a mutant SOD1 gene. Brain Res 1150:182–189.

Nagakubo D, Taira T, Kitaura H, Ikeda M, Tamai K, Iguchi-Ariga SM, Ariga H. 1997. DJ-1, a novel oncogene which transforms mouse NIH3T3 cells in cooperation with ras. Biochem Biophys Res Commun 231:509–513.

Nair VD, McNaught KS, Gonzalez-Maeso J, Sealfon SC, Olanow CW. 2006. p53 mediates nontranscriptional cell death in dopaminergic cells in response to proteasome inhibition. J Biol Chem 281:39550–39560.

Ohta Y, Nagai M, Nagata T, Murakami T, Nagano I, Narai H, Kurata T, Shiote M, Shoji M, Abe K. 2006. Intrathecal injection of epidermal growth factor and fibroblast growth factor 2 promotes proliferation of neural precursor cells in the spinal cords of mice with mutant human SOD1 gene. J Neurosci Res 84:980–992.

Prives C, Hall PA. 1999. The p53 pathway. J Pathol 187:112–126.

Rosen DR, Siddique T, Patterson D, Figlewicz DA, Sapp P, Hentati A, Donaldson D, Goto J, O'Regan JP, Deng HX. 1993. Mutations in Cu/Zn superoxide dismutase gene are associated with familial amyotrophic lateral sclerosis. Nature 362:59–62.

Sakurai M, Kawamura T, Nishimura H, Suzuki H, Tezuka F, Abe K. 2009. Induction of Parkinson disease-related proteins in motor neurons after transient spinal cord ischemia in rabbits. J Cereb Blood Flow Metab 29:752–758.

Sasaki S, Tsutsumi Y, Yamane K, Sakuma H, Maruyama S. 1992. Sporadic amyotrophic lateral sclerosis with extensive neurological involvement. Acta Neuropathol 84:211–215.

Sasaki S, Aoki M, Nagai M, Kobayashi M, Itoyama Y. 2009. Mitochondrial alterations in transgenic mice with an H46R mutant Cu/Zn superoxide dismutase gene. J Neuropathol Exp Neurol 68:365–373.

Schapira AH. 2008. Mitochondria in the aetiology and pathogenesis of Parkinson's disease. Lancet Neurol 7:97–109.

Shaulsky G, Goldfinger N, Tosky MS, Levine AJ, Rotter V. 1991. Nuclear localization is essential for the activity of p53 protein. Oncogene 6:2055–2065.

Shieh SY, Ikeda M, Taya Y, Prives C. 1997. DNA damage-induced phosphorylation of p53 alleviates inhibition by MDM2. Cell 91:325–334.

Shimizu M, Miyazaki I, Higashi Y, Eslava-Alva MJ, Diaz-Corrales FJ, Asanuma M, Ogawa N. 2008. Specific induction of PAG608 in cranial and spinal motor neurons of L-DOPA-treated parkinsonian rats. Neurosci Res 60:355–363.

Tomasevic G, Shamloo M, Israeli D, Wieloch T. 1999. Activation of p53 and its target genes p21(WAF1/Cip1) and PAG608/Wig-1 in ischemic preconditioning. Brain Res Mol Brain Res 70:304–313.

Tsuboi Y, Munemoto H, Ishikawa S, Matsumoto K, Iguchi-Ariga SM, Ariga H. 2008. DJ-1, a causative gene product of a familial form of Parkinson's disease, is secreted through microdomains. FEBS Lett 582:2643–2649.

Valente EM, Abou-Sleiman PM, Caputo V, Muqit MM, Harvey K, Gispert S, Ali Z, Del Turco D, Bentivoglio AR, Healy DG, Albanese A, Nussbaum R, Gonzalez-Maldonado R, Deller T, Salvi S, Cortelli P, Gilks WP, Latchman DS, Harvey RJ, Dallapiccola B, Auburger G, Wood NW. 2004. Hereditary early-onset Parkinson's disease caused by mutations in PINK1. Science 304:1158–1160.

Vargas MR, Pehar M, Cassina P, Beckman JS, Barbeito L. 2006. Increased glutathione biosynthesis by Nrf2 activation in astrocytes prevents p75NTR-dependent motor neuron apoptosis. J Neurochem 97:687–696.

Vanneh-Ziaie S, Okan I, Wang Y, Magnusson KP, Warthoe P, Strauss M, Wiman KG. 1997. Wig-1, a new p53-induced gene encoding a zinc finger protein. Oncogene 15:2699–2704.

Warita H, Hayashi T, Murakami T, Manabe Y, Abe K. 2001. Oxidative damage to mitochondrial DNA in spinal motoneurons of transgenic ALS mice. Brain Res Mol Brain Res 89:147–152.

Wong PC, Pardo CA, Borchelt DR, Lee MK, Copeland NG, Jenkins NA, Sisodia SS, Cleveland DW, Price DL. 1995. An adverse property of a familial ALS-linked SOD1 mutation causes motor neuron disease characterized by vacuolar degeneration of mitochondria. Neuron 14:1105–1116.

Yanagisawa D, Kitamura Y, Inden M, Takata K, Taniguchi T, Morikawa S, Morita M, Inubushi T, Tooyama I, Taira T, Iguchi-Ariga SM, Akaike A, Ariga H. 2008. DJ-1 protects against neurodegeneration caused by focal cerebral ischemia and reperfusion in rats. J Cereb Blood Flow Metab 28:563–578.

# Familiar amyotrophic lateral sclerosis (FALS)-linked SOD1 mutation accelerates neuronal cell death by activating cleavage of caspase-4 under ER stress in an *in vitro* model of FALS

Yoshihisa Koyama [a,1], Toru Hiratsuka [a,1], Shinsuke Matsuzaki [a,b,1], Satoru Yamagishi [a], Shinsuke Kato [c], Taiichi Katayama [b,*], Masaya Tohyama [a,b]

[a] Department of Anatomy and Neuroscience, Graduate School of Medicine, Osaka University, 2-2 Yamadaoka, Suita, Osaka 565-0871, Japan
[b] Department of Child Development and Molecular Brain Science, United Graduate School of Child Development, Osaka University, Kanazawa University and Hamamatsu University School of Medicine, 2-2 Yamadaoka, Suita, Osaka 565-0871, Japan
[c] Department of Neuropathology, Institute of Neurological Sciences, Faculty of Medicine, Tottori University, Yonago, Tottori 683-8503, Japan

## ARTICLE INFO

## ABSTRACT

Recently, endoplasmic reticulum (ER) dysfunction has been implicated in the pathogenesis of familial amyotrophic lateral sclerosis (FALS). Although up-regulation of caspase-12 has been reported in G93A SOD1 transgenic mice, it is controversial whether similar mechanisms operate in human FALS. We found that ER stress in cells stably expressing L84V SOD1 induces neuronal cell death and accelerates cleavage of caspase-4. We also detected oligomer formation of L84V SOD1 in L84V SOD1-expressing human neuroblastoma cells. These findings show that ER stress in L84V SOD1-expressing human cells causes the aggregation and inclusion bodies of L84V SOD1 to induce neuronal death through the accelerated cleavage of caspase-4.

© 2010 Elsevier Ltd. All rights reserved.

## 1. Introduction

Amyotrophic lateral sclerosis (ALS) is a neurodegenerative disorder, clinically characterized by progressive dysfunction of either upper or lower limb, beginning in middle age. Pathologically, severe motor neuronal loss is found in the ALS spinal cord. About 10% of cases of ALS are inherited, usually as autosomal dominant trait, a disorder known as familiar ALS (FALS) (Gurney, 2000; Brown and Robberecht, 2001; Cleveland and Rothstein, 2001; Rowland and Schneider, 2001; Bruijin et al., 2004). More than 20% of FALS cases are associated with mutation of the Cu/Zn-superoxide dismutase (SOD) (Rosen et al., 1993). Nearly 100 different mutations in the SOD1 gene have been identified in FALS patients. Neuronal Lewy body-like hyaline inclusions (LBHI) containing mutant SOD1 are morphological hallmarks of FALS associated with mutant SOD1, although little is known about the formation of LBHI in neurons (Bruijin et al., 2004). We recently reported that ER stress induces the appearance of LBHI-like inclusions (LBHI-I) in human neuroblastoma (SK-N-SH) cells expressing SOD1 with the L84V (L84V SOD1) mutation associated

with FALS (Yamagishi et al., 2007). These LBHI-I closely resemble LBHI in patients with SOD1-linked FALS, because LBHI-I and LBHI share the similar cytological and immunohistochemical characteristics (Yamagishi et al., 2007). Furthermore, there is evidence demonstrating that ER stress plays an important role in the pathogenesis of FALS. Up-regulation of Bip in the spinal motor neurons of H46R (H46R SOD1) and L84V SOD1 transgenic mice (Tobisawa et al., 2003; Atkin et al., 2006), and up-regulation of the ER-resident protein disulfide isomerase (PDI) family members in the lumbar spinal cords of G93A SOD1 transgenic mice (Wate et al., 2005) have been reported. Moreover, Ilieva et al. reported that oxydative and ER stress interplay in sporadic ALS (Ilieva et al., 2007). Based upon these findings, it is likely that the LBHI seen in human patients with mutant SOD1-linked FALS arise from ER dysfunction.

On the other hand, we have shown that familial AD (FAD)-linked PS1 mutations increase vulnerability to ER by altering the unfolded-protein response (UPR) (Katayama et al., 1999; Sato et al., 2001). Although caspase-12 has been shown to be involved in signaling pathways specific to ER stress-induced apoptosis in rodents (Nakagawa et al., 2000), caspase-12 protein is not produced in humans (Fischer et al., 2002). Accordingly, caspase-12 does not function in ER stress-induced apoptosis associated with FAD. Recently, we revealed that FAD-linked PS1 mutation accelerates the cleavage of caspase-4 under ER stress to induce

neuronal cell death (Hitomi et al., 2004; Yukioka et al., 2008). However, it is still unclear whether ER stress causes neuronal death in FALS. Although up-regulation of caspase-12 in G93A SOD1 mice has been reported (Wootz et al., 2004), direct evidence indicating that ER stress causes neuronal death, and that, as has been demonstrated in FAD, caspase-4 can function as an ER stress-induced caspase and is involved in the pathogenesis of FALS, is lacking. In the present study, using an *in vitro* model for FALS (L84V-expressing human neuroblastoma cells), we found that the L84V SOD1 mutation accelerates cleavage of caspase-4 to induce neuronal death under conditions of ER stress, that ER stress in L84V SOD1-expressing cells causes oligomer formation by L84V SOD1, and that ER stress in these cells increases the number of LBHI-I exhibiting SOD1 and ubiquitin immunoreactivity. This suggests that ER stress in L84V SOD1-expressing human cells causes the aggregation of L84V SOD1 in the inclusion bodies to induce neuronal death.

## 2. Results

### 2.1. L84V SOD1 mutation increases vulnerability to ER stress

Before examining the effect of L84V SOD1 mutation on ER stress-induced cell death, we generated SK-N-SH human neuroblastoma cell lines that stably express FLAG-tagged human L84V SOD1 mutation associated with FALS (Aoki et al., 1995). Western blot analysis confirmed that expression of endogenous and exogenous SOD1 was equal in the cell line (Yamagishi et al., 2007). We then added tunicamycin (TM), which induces ER stress by preventing protein glycosylation, to the medium. After the TM treatment, cell death increased in cells expressing L84V SOD1 compared with cells expressing the wild-type protein (Fig. 1A). On the other hand, the increase in cell death induced by hydrogen peroxide (data not shown) or staurosporine was not affected by expression of L84V SOD1 (Fig. 1B). These findings showed that the L84V SOD1 mutation increases vulnerability to ER stress.

Next we examined the effect of L84V SOD1 on ER stress-induced apoptosis at the morphological level 9.5 h after TM stimulation (Fig. 1C–H). Assessment of cell death was performed using a terminal deoxynucleotidyl transferase (TdT) dUTP nick-end labeling (TUNEL) method with an ApoTag *in situ* apoptosis detection kit (Oncor). As a result, TUNEL-positive cells were detected in both wild-type and L84V SOD1 cells 9.5 h after TM treatment (Fig. 1C), and the ratio of TUNEL-positive cells to total cells was significantly increased in L84V SOD1-expressing cells (to over 33%) more than in cells expressing wild-type SOD1 (Fig. 1D) 9.5 h after TM treatment. Moreover, to confirm that L84V SOD1 cells also undergo apoptosis morphologically, identification of apoptotic L84V SOD1 cells by hematoxylin–eosin (HE) staining was performed (Fig. 1E). Fig. 1E shows a representative apoptotic cell expressing L84V SOD1 with eosinophilic staining (Fig. 1E, arrow). Subsequent ultrastructural analysis of an apoptotic L84V SOD1 cell identified by HE staining, by electron microscopy, also showed that these cells exhibited typical apoptotic morphological changes, including nuclear fragmentation, chromatin condensation (Fig. 1F and H, arrows), the appearance of many vacuoles (Fig. 1F, arrow heads) and cell shrinkage. Surprisingly, electron microscopic analysis revealed ER located at the periphery of the cytoplasm of apoptotic cells, namely eosinophilic apoptotic bodies (Fig. 1F and G, arrows).

Thus, these results revealed that the L84V SOD1 mutation specifically increases vulnerability to ER stress and cell death by apoptosis.

### 2.2. L84V SOD1 mutation accelerates the cleavage of caspase-4 under ER stress

To examine whether caspase-4 was specifically cleaved from L84V SOD1-expressing cells under ER stress, we compared the cleavage of caspase-4 between L84V SOD1 and wild-type SOD1-expressing cells under TM treatment, and we also compared the cleavage of caspase-4 in cells expressing L84V SOD1 with and without TM treatment. In the wild-type SOD1 cells, final cleavage products of procaspase-4 (Fig. 2A, left panel arrow) could not be detected under the basal condition, and increased gradually after the addition of TM (Fig. 2A, left panel). In the cells expressing L84V SOD1, the cleaved form of caspase-4 was detected in the basal condition (Fig. 2A, right). L84V SOD1 expression increased the cleavage of procaspase-4 time-dependently under TM treatment, compared with that found in cells expressing wild-type SOD1 (Fig. 2A, right). In contrast, when cells expressing L84V SOD1 were exposed to non-ER stress, staurosporine at a dose providing a similar extent of cell death to that induced by TM, final cleavage products of procaspase-4 were not observed (Fig. 2B). Densitometric analyses of cleaved-caspase-4 revealed a significant difference between wild-type SOD1-expressing cells and L84V SOD1-expressing cells at 3 and 6 h after TM treatment (Fig. 2C).

### 2.3. ER stress accelerates the aggregation of L84V SOD1 under ER stress

To determine the state of aggregated mutant SOD1 in the inclusion body, we applied native-polyacrylamide gel electrophoresis (native-PAGE) to L84V and wild-type SOD1-expressing SK-N-SH cells treated with TM.

Comparing the position of wild-type SOD1 after TM treatment on the gel with those of protein makers, a single thick band at an apparent molecular weight of about 15 kDa, corresponding to the molecular weight of SOD1, was found, but no oligomer formation by denatured wild-type SOD1 was detected (Fig. 2D, SOD1$^{WT}$). On the other hand, when L84V SOD1 was examined, oligomers of L84V SOD1 were observed (Fig. 2D, SOD1$^{L84V}$). Judging from the molecular weights and specificity of SOD-positive bands by Western blot analysis, these bands likely represent dimers, trimers and higher molecular weight oligomers of L84V SOD1 (Fig. 2D, SOD1$^{L84V}$).

## 3. Discussion

### 3.1. L84V SOD1 mutation increases vulnerability to ER stress

If LBHI-I is associated with the pathogenesis of ALS, cells with LBHI-I would be vulnerable like the motor neurons in the spinal cords of ALS patients and SOD1 mutant transgenic mice. However, it has been unclear whether our human neuroblastoma cells expressing L84V SOD1, which have LBHI-I, are more vulnerable to ER stress than wild-type SOD1-expressing cells. We performed a cell death assay using cells expressing L84V SOD1 and wild-type SOD1. Cell death increased in cells expressing L84V SOD1 compared with cells expressing the wild-type protein. ER stress is suspected to be involved in the neuronal death occurring in various neurodegenerative diseases, such as Alzheimer's disease (AD) (Katayama et al., 1999; Sato et al., 2001), ischemia (Bando et al., 2003), Huntington's disease (Kouroku et al., 2002), ALS (Kanekura et al., 2009) and Parkinson's disease (Ryu et al., 2002). Regarding the pathogenesis of FALS, neuronal LBHI seen in a human patient with L84V SOD1-linked FALS were shown to be caused by ER dysfunction in human neuroblastoma cells and L84V SOD1 transgenic mice (Yamagishi et al., 2007), and significant up-regulation of the ER-resident protein disulfide isomerase (PDI)

family members was shown in the lumbar spinal cord of transgenic G93A SOD1 model mice for FALS (Atkin et al., 2006). In this experiment, aggregates of SOD1 and formation of LBHI-I were shown in L84V SOD1-expressing cells, induced by ER stress, as we had shown in a previous study. Prolonged ER stress subsequently activated the apoptotic pathway, resulting in cell death. We analyzed activation of caspase-4 in these cells. As expected, the SOD aggregates of L84V SOD1-expressing cells colocalized with caspase-4. Indeed, apoptotic morphological changes were ob-

served in cells with SOD aggregates; however, we detected no activation of caspase-4 in cells with LBHI-I (data not shown). Therefore, caspase-4 is associated with aggregation, but inclusions are not directly related to caspase-4 activation. At any rate, the present study showed that the L84V SOD1 mutation expressed in FALS increases neuronal vulnerability to ER stress. Thus, the ER may be important for regulating intracellular apoptotic signaling in neurons of FALS patients, as has been revealed in AD, ischemia, Parkinson's disease and Huntington's disease.
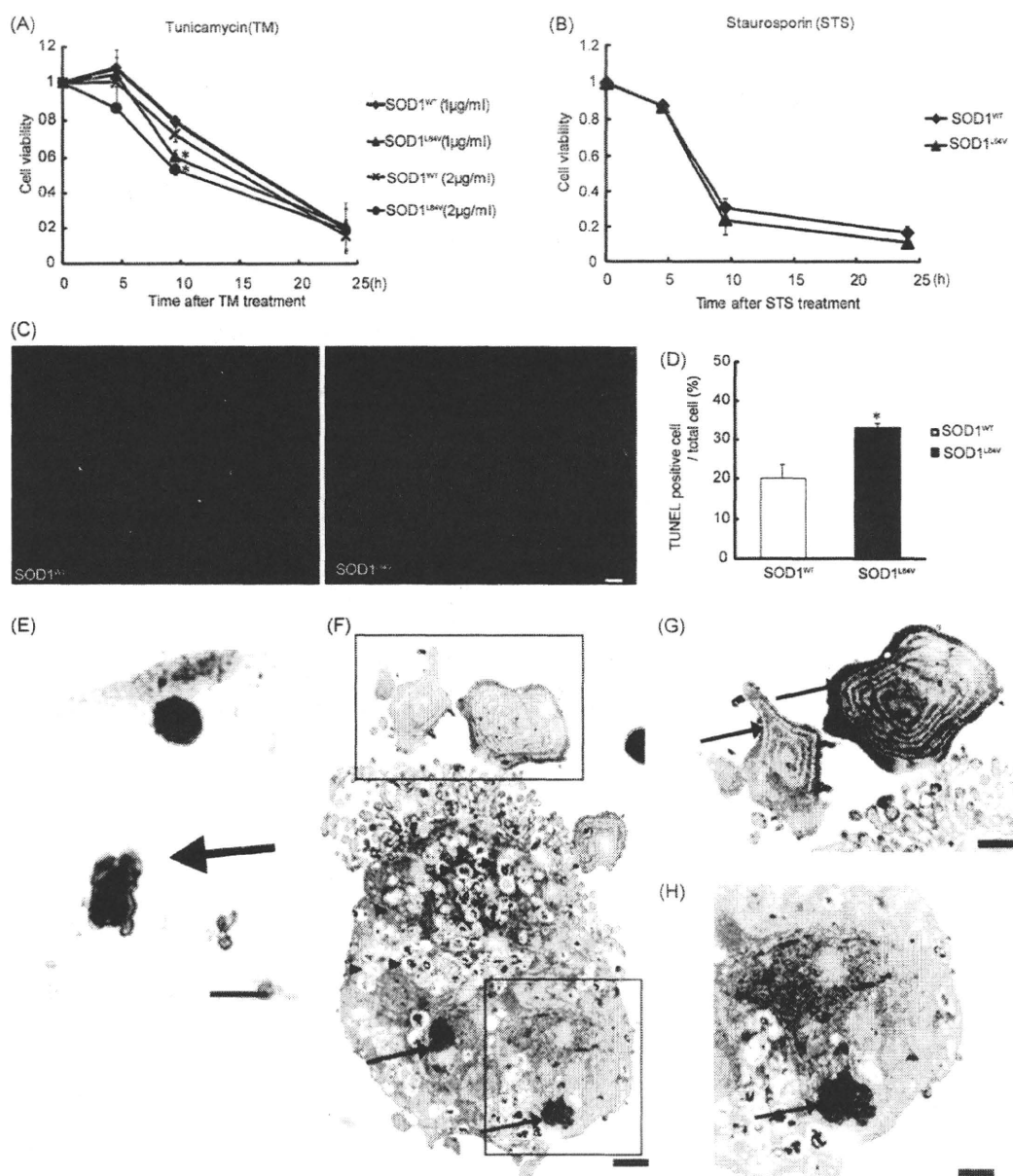


Fig. 1. L84V SOD1 mutation alters sensitivity to ER stress. Cell viability of both wild-type and L84V SOD1-expressing cells for the indicated period after 1 or 2 μg/ml tunicamycin (TM) treatment using the WST-1 activity assay (A), or after 0.5 μM staurosporine treatment using an assay based on the morphological change (B). These data represent the means ± S.E.M. of five independent experiments. Asterisks show a significant difference from wild-type SOD1 (SOD1$^{WT}$). Asterisks indicate $P < 0.01$ by the Student's $t$-test. (C) The L84V SOD1 mutation expression accelerates apoptosis 9.5 h after TM treatment. Significantly more TUNEL-positive nuclei are observed in L84V SOD1-expressing cells (left panel) than in wild-type SOD1-expressing cells (right panel) under TM treatment. Scale bar = 50 μm. (D) The extent of cell death assessed by TUNEL staining, and expressed as the means ± S.E.M. of three independent experiments. Asterisks show a significant difference from wild-type SOD1. Asterisks indicate $P < 0.01$. (E) Identification of the apoptotic L84V SOD1-expressing cells (arrow) under TM stimulation using hematoxylin–eosin (HE) staining at the light microscopic level. Scale bar = 100 μm. (F) Electron microscopy showing the apoptotic L84V SOD1-expressing cells after TM treatment. A number of vacuoles (arrow head), chromatin condensation and nuclear fragmentation (arrow) are seen. Eosinophilic apoptotic bodies contained ER, which shows an aberrant distribution (G; enlargement of the upper square in (F), arrow) and chromatin condensation (H; enlargement of the lower square in (F), arrow) at the higher magnification. Scale bar = 10 μm (F) and 5 μm (G and H).
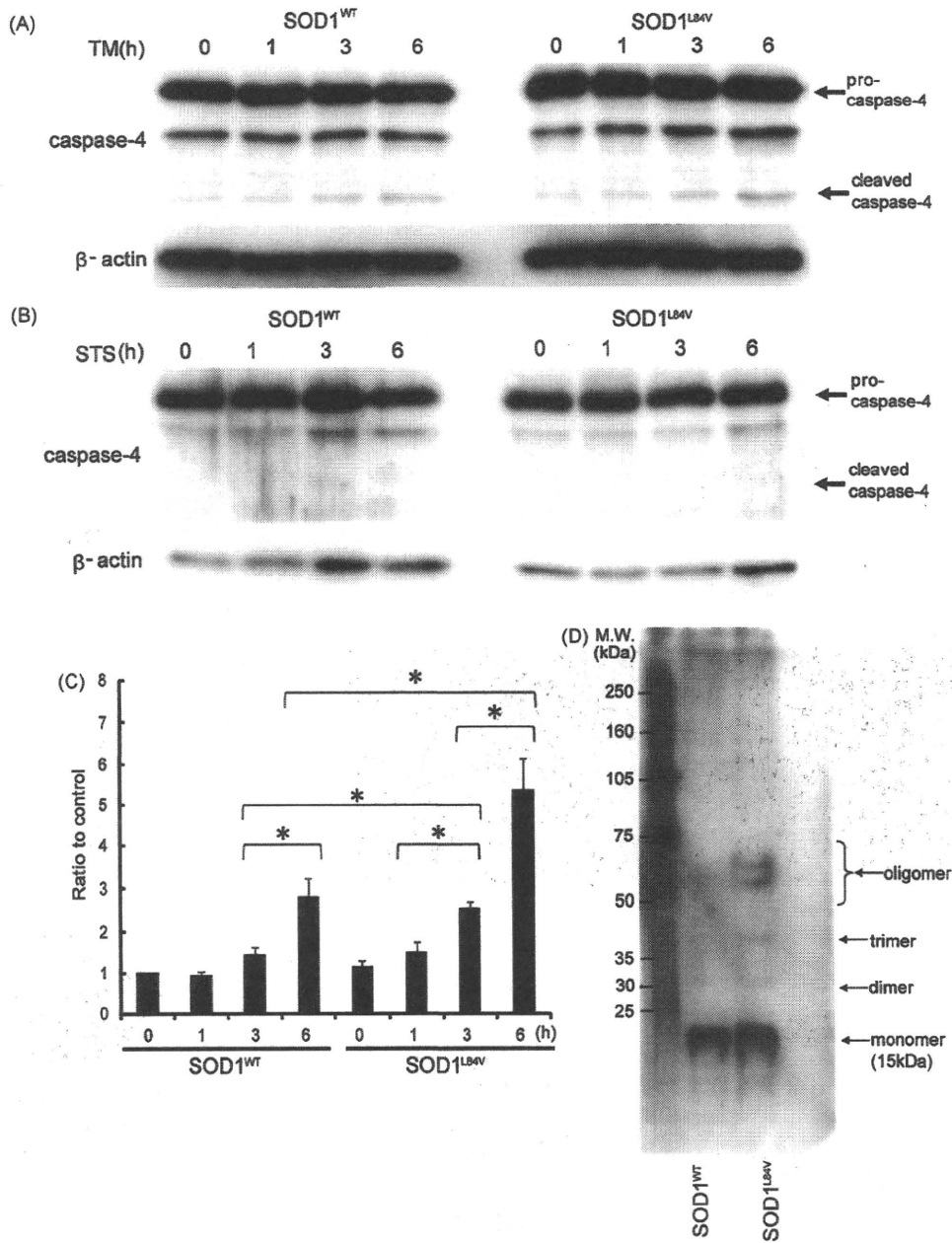
**Fig. 2.** L84V SOD1 accelerates the cleavage of caspase-4 under ER stress. SK-N-SH cells stably expressing wild-type SOD1 (SOD1$^{WT}$) (A, left panel) and L84V SOD1 mutation (SOD1$^{L84V}$) (A, right panel) were treated with 1 μg/ml tunicamycin (TM) followed by incubation for the indicated periods. (B) Non-ER stress. Staurosporine does not induce an increase in the cleavage of caspase-4. Equal amounts of cell lysates were analyzed by Western blotting using anti-caspase-4 and β-actin antibody. (C) Densitometric analyses of Western blot results (A). *$P < 0.01$ for comparison with wild-type SOD1 cells, by the Student's $t$-test. (D) Oligomer formation by SOD1 protein in both wild-type and L84V SOD1-expressing cells at 21 h after 1 μg/ml TM treatment using native-PAGE. M.W., molecular weight marker. The volume of loaded markers was 5 μl. The quantity of protein was 15–25 μg.

### 3.2. L84V SOD1 mutation accelerates the cleavage of caspase-4 under ER stress

In rodents, caspase-12 mediates apoptosis specifically in response to ER stress (Nakagawa et al., 2000). A significant up-regulation of caspase-12 was also observed in transgenic G93A SOD1 ALS model mice (Atkin et al., 2006). However, caspase-12 protein is not produced in humans, because the gene is interrupted by a frame shift and premature stop codon; there is also an amino acid substitution in the critical site for caspase activity in humans (Fischer et al., 2002). Therefore, some other caspases with similar

structure might substitute functionally for caspase-12 in humans. We have found that caspase-4 can function as an ER stress-induced caspase in humans (Hitomi et al., 2004). Subsequently, we have revealed that caspase-4 is involved in pathogenesis of AD, because a familial AD-linked mutation enhances the cleavage of caspase-4 (Yukioka et al., 2008). The present study demonstrated that a FALS-linked mutation (L84V SOD1 mutation) enhances the cleavage of caspase-4, suggesting that caspase-4 might play a key role in the pathogenesis of FALS.

Thus, caspase-4 is a key caspase for neuronal death in both AD and FALS, suggesting that cleavage of procaspase-4 may induce the

neuronal cell death in ischemia, Parkinson's disease and Huntington's disease, because dysfunction of the ER causes the neuronal death in these diseases.

### 3.3. ER stress accelerates the aggregation of L84V SOD1 under ER stress

While the importance of ER stress or proteasome malfunction in the formation of mutant SOD1 aggregation has been suggested (Kato et al., 2000; Johnston et al., 2000; Julien, 2001; Hyun et al., 2003; Tobisawa et al., 2003; Kikuchi et al., 2006), the mechanism by which mutant SOD1 forms LBHI in FALS remains unclear. In this study using SK-N-SH cells, it is shown that mutant SOD1, but not the wild-type SOD1, forms oligomers under ER stress conditions. Thus, it is likely that ER stress to SK-N-SH cells expressing L84V SOD1 results in the formation of SOD1- and ubiquitin-immunoreactive inclusion bodies, which contain ER and oligomerized mutant SOD1. Because inclusion bodies with a similar character were observed in the motor neurons of L84V SOD1 transgenic mice, ER stress to neurons expressing mutant SOD1 produces LBHI composed of ER and oligomerized mutant SOD1, which induces the cell death. However, it remains unclear why the same type of stress induces different outcomes for mutant SOD1 aggregation in neuroblastoma cells. Alternatively, there are various reports about the relation between pathogenesis of ALS and the inclusion body of ALS so far. For example, it is known that protein TDP-43 is a component of ubiquitin-positive, tau-negative inclusions, that is different from SOD-positive inclusions (Arai et al., 2006; Mackenzie et al., 2007). Moreover, it was reported that organelle-derived inclusion bodies are associated with neurodegenerative diseases (Okado-Matsumoto and Fridovich, 2001; Sturtz et al., 2001; Nishimura et al., 2004; Kanekura et al., 2006; Filimonenko et al., 2007). Thus, to address above issue, we should obtain much more evidence related to ER function and the formation of aggregates. To date, we have found common features between the small aggregates in L84V SOD1-expressing SK-N-SH cells and neuronal LBHI-precursor in L84V transgenic mice, including regions of abnormal ER aggregation surrounded by abundant free ribosomes. Furthermore, in accordance with the findings of our previous study (Yamagishi et al., 2007), exposure to TM resulted in the development of a number of eosinophilic aggregates and inclusion bodies at the periphery of the cytoplasm of L84V SOD1-expressing SK-N-SH human neuroblastoma cells, but not in cells expressing wild-type SOD1. The aggregates and inclusion bodies were positive also for SOD1, ubiquitin, an ER retention signal (KEDL) protein and Bip (data not shown, see Yamagishi et al., 2007), showing that L84V SOD1 is localized in the aggregates, inclusion bodies and ER. Subsequent electron microscopic analysis revealed that eosinophilic aggregates and the inclusion bodies located at the periphery of the cytoplasm contained ER (data not shown) as described in our previous study (Yamagishi et al., 2007).

Thus, the results revealed that the L84V SOD1 mutation increases vulnerability to ER stress and the appearance of aggregates and inclusion bodies containing L84V SOD1 and ER. In conclusion, our *in vitro* model might shed light on the development of therapies that can prevent the progression of mutant SOD1-linked FALS.

## 4. Experimental procedures

### 4.1. Cell culture

Non-differentiated SK-N-SH human neuroblastoma cells were obtained from the Riken Cell Bank (Tsukuba, Japan), and were cultured in α-MEM (Invitrogen) containing 10% fetal bovine serum at 37 °C under 5% $CO_2$. These cells were transfected with pcDNA3.1-hSOD1 and pcDNA3.1-hL84V-SOD1 to cause over-expression of wild-type or L84V mutant SOD1, respectively. G418-resistant stable neuroblastoma cell lines expressing equal levels of endogenous and exogenous SOD1 were established. In all experiments, we used cultures that were at 70–80%

confluence to avoid the influence of stress induced by overgrowth. On the day of stimulation, fresh medium was added more than 1 h before exposure to stress to ensure the same conditions for each culture.

### 4.2. Cell viability assay

#### 4.2.1. WST-1 activity assay

L84V SOD1-expressing or WT cells ($3 \times 10^3$) were plated onto a 96-well plate 36 h before the cell viability assay. Cells were treated with 1 or 2 μg/ml TM for the indicated periods shown in Fig. 1A, and 10 μl of WST-1 (Roche, Basel, Switzerland) was added to the medium and cultured for 3 h. Signal for WST-1 was determined by the absorption at a wavelength of 450–650 nm. Data are expressed as the means ± standard errors of the means (S.E.M.) for at least three independent experiments.

#### 4.2.2. Assay based on the morphological change

Cell toxicity to WT cells and L84V cells treated with 40 and 80 μM $H_2O_2$ or 0.5 μM staurosporine for the indicated periods shown in Fig. 1B was assessed as follows. Cell death was evaluated on the basis of morphological changes observed by phase contrast microscopy or nuclear changes fluoroscopically detected after costaining the cells with 10 μM Hoechst 33342 and 10 μM propidium iodide (PI). Nuclear fragmentation was detected by Hoechst-positive staining and nuclear collapse was detected by PI-positive staining. Dead cells were identified on the basis of being double-positive. The staining was measured independently in three fields and at least 300 cells were counted. Data are expressed as the means ± S.E.M. for at least three independent experiments.

### 4.3. In situ detection of apoptosis

*In situ* detection of apoptotic cells was performed using a TUNEL method with a TMR red *in situ* cell death detection kit (Roche). Briefly, cells were washed in 0.1 M phosphate-buffered saline (PBS), fixed at room temperature (RT) for 1 h in 0.1 M PBS containing 4% paraformaldehyde (PFA), blocked with 0.1% sodium citrate buffer containing 0.1% Triton X for 2 min on ice, and incubated at 37 °C for 1 h with 50 μl of TUNEL reaction buffer from the Roche kit. The apoptotic cells were labeled with red fluorescent dye and counted using a fluorescence microscope. TUNEL-positive cells were expressed as a percentage of total cells. For each experiment, a minimum of five fields was examined.

### 4.4. Immunohistochemistry

Non-differentiated SK-N-SH cells stably expressing wild-type SOD1 or L84V SOD1 were treated with 1 or 2 μg/ml of TM for 24 h. Then, the cells were fixed with Zamboni's solution, rinsed in 0.1 M PBS, and incubated for 30 min in 0.3% $H_2O_2$ to eliminate endogenous peroxidases. Next, the cells were incubated overnight at 4 °C with an anti-SOD1 antibody (1:1000 dilution) (Chemicon, Temecula, CA), anti-KDEL antibody (1:500 dilution) (Stressgen, Victoria, BC, Canada) or anti-ubiquitin antibody (1:500 dilution) (Stressgen, Victoria, BC, Canada) in 0.1 M PBS containing 0.3% Triton X-100 and 3% bovine serum albumin (BSA). After washing in 0.1 M PBS, cells for detection of SOD1 were incubated for 30 min with biotinylated anti-sheep IgG (Vector Laboratories, Burlingame, CA). Following amplification with avidin–biotin complex from the ABC kit (Vector Laboratories), reaction products were visualized with 0.05 M Tris–HCl buffer containing 0.02% diaminobenzidine (DAB) and 0.1% hydrogen peroxide. Cells positive for KDEL or ubiquitin were incubated with fluorescent dye (Alexa Fluor 568)-conjugated goat anti-mouse IgG (for KDEL, 1:1000 dilution) or goat anti-rabbit IgG (for ubiquitin, 1:1000 dilution) (Molecular Probes, Eugene, OR) for 1 h at room temperature in 0.02 M PBS containing 3% BSA. Finally, the cells were counterstained with hematoxylin and eosin.

### 4.5. Electron microscopy

Wild-type or L84V SOD1-expressing cells were exposed to 1 μg/ml TM for 24 h and then fixed at RT for 1 h in 0.1 M phosphate buffer (PB) containing 2.5% glutaraldehyde and 2% PFA. After apoptotic L84V SOD1-expressing cells were identified by Mayer's hematoxylin and eosin (HE) staining, they were decolorized, rehydrated and rinsed in 0.1 M PB. Thereafter, the cells were post-fixed in 1% $OsO_4$ at RT for 1 h, dehydrated in a graded ethanol series, and embedded in epon resin (Quetol 812; Nisshin EM Co.). Areas containing apoptotic cells were block-mounted in epoxy-resin by the direct epoxy-resin embedding method (Yamagishi et al., 2007) and cut into 80-nm sections. The sections were counterstained with uranyl acetate and lead citrate and then examined using an H-7100 electron microscope (Hitachi).

### 4.6. Western blot analysis

Wild-type or L84V SOD1-expressing cells were harvested at 0, 1, 3 and 6 h after addition of 1 μg/ml TM, 40 and 80 μM $H_2O_2$ or 0.5 μM staurosporine, and then lysed in TNE buffer (50 mM Tris–HCl (pH 7.5), 1 mM EDTA (pH 8.0), 150 mM NaCl) containing 0.5% NP40. Protein samples (20 μg) were subjected to 12% SDS-PAGE and transferred to polyvinylidene difluoride filters (Millipore, Bedford, MA). The membranes were blocked with 0.1 M PBS containing 5% skim milk and 0.05%

Tween20 for 1 h at RT and incubated overnight at 4 °C with a mouse monoclonal anti-caspase-4 primary antibody (1:1000; MBL, Raleigh, NC). After washing in 0.1 M PBS containing 0.05% Tween20, the membranes were then incubated for 1 h at RT with a HRP conjugated anti-mouse IgG secondary antibody (1:2000; Cell Signaling, Beverly, MA), visualized in ECL solution (GE Healthcare Bio-Sciences Corporation, Piscataway, NJ, USA) for 1 min, and exposed onto X-Omat film (FUJI, Kanagawa, Japan) for 1–3 min. Finally, the membranes were incubated in a stripping buffer (2% SDS, 0.7% β-mercaptoethanol, 62.5 mM Tris–HCl, pH 6.8) for 30 min at 65 °C and re-probed with a monoclonal mouse anti-β-actin (1:3000; Chemicon, Rosmont, IL) primary antibody and a HRP conjugated anti-mouse IgG secondary antibody as loading controls. Our Western blot bands showed the same band sizes as indicated in the antibody information sheets. Each protein level was quantified by densitometry (Image J, National Institutes of Health, USA) and normalized to the β-actin levels.

### 4.7. Native-polyacrylamide gel electrophoresis

Native-PAGE was performed as reported previously (Schagger, 2006; Wittig et al., 2006). Membrane protein (30–100 μg protein per gel lane) was resuspended in 0.2–0.5% n-dodecyl β-ᴅ-maltoside (DDM) (or alternate treatment as indicated) in buffer composed of 50 mM NaCl, 5 mM 6-aminohexanoic acid and 50 mM imidazole pH 7.0 and then clarified after 15 min at room temperature by microcentrifuge centrifugation for 5 min before addition of 0.5% Coomassie G250 (Sigma) and 50 mM 6-aminohexanoic acid. Samples were resolved on 4–16.5% gradient acrylamide gels with cooling; the anode buffer contained 25 mM imidazole pH 7.0 and the cathode buffer contained 50 mM tricine, 7.5 mM imidazole pH 7.0 with 0.02% Coomassie G250. High molecular mass standards for native electrophoresis were obtained from Amersham and were stained with Coomassie R250. Wild-type SOD1 and L84V SOD1 after 1 μg/ml of TM stimulation for 24 h were loaded onto a gel. Following electrophoretic transfer to a PVDF membrane (Immobilon-P, Millipore), proteins were identified by immunoblotting and detection with ECL as described above (see Section 4.6).

### Acknowledgment

### References

Arai, T., Hasegawa, M., Akiyama, H., Ikeda, K., Nonaka, T., Mori, H., Mann, D., Tsuchiya, K., Yoshida, M., Hashizume, Y., Oda, T., 2006. TDP-43 is a component of ubiquitin-positive tau-negative inclusions in frontotemporal lobar degeneration and amyotrophic lateral sclerosis. Biochem. Biophys. Res. Commun. 351, 602–611.

Atkin, J.D., Farg, M.D., Turner, B.J., Tomas, D., Lysaght, J.A., Nunan, J., Rembach, A., Nagley, P., Beart, P., Cheema, S.S., Horne, M.K., 2006. Induction of the unfolded protein response in familial amyotrophic lateral sclerosis and association of protein-disulfide isomerase with superoxide dismutase 1. J. Biol. Chem. 281, 30152–30165.

Aoki, M., Abe, K., Houi, K., Ogasawara, M., Matsubara, Y., et al., 1995. Variance of age at onset in a Japanese family with amyotrophic lateral sclerosis associated with a novel Cu/Zn superoxide dismutase mutation. Ann. Neurol. 37, 676–679.

Bando, Y., Katayama, T., Kasai, K., Taniguchi, M., Tamatani, M., Tohyama, M., 2003. GRP94 (94 kDa glucose-regulated protein) suppresses ischemic neuronal death against ischemia/reperfusion injury. Eur. J. Neurosci. 18, 829–840.

Bruijin, L.I., Miller, T.M., Cleveland, D.W., 2004. Unraveling the mechanism involved in motor neuron degeneration in ALS. Annu. Rev. Neurosci. 27, 723–749.

Brown Jr., R.H., Robberecht, W., 2001. Amyotrophic lateral sclerosis: pathogenesis. Semin. Neurol. 21, 131–139.

Cleveland, D.W., Rothstein, J.D., 2001. Deciphering selective motor neuron death in ALS. In: From Charcot to Lou Gehrig. Nat. Rev. Neurosci. 2, 806–819.

Filimonenko, M., Stuffers, S., Raiborg, C., Yamamoto, A., Malerød, L., Fisher, E.M., Isaacs, A., Brech, A., Stenmark, H., Simonsen, A., 2007. Functional multivesicular bodies are required for autophagic clearance of protein aggregates associated with neurodegenerative disease. J. Cell Biol. 179, 485–500.

Fischer, H., Koenig, U., Eckhart, L., Tschachler, E., 2002. Human caspase-12 acquired deleterious mutations. Biochem. Biophys. Res. Commun. 293, 722–726.

Gurney, M.E., 2000. What transgenic mice tell us about neurodegenerative disease. Bioessays 22, 297–304.

Hitomi, J., Katayama, T., Eguchi, Y., Kudo, T., Taniguchi, M., Koyama, Y., Manabe, T., Yamagishi, S., Bando, Y., Imaizumi, K., Tsujimoto, Y., Tohyama, M., 2004. Involvement of caspase-4 in endoplasmic reticulum stress-induced apoptosis and Aβ-induced cell death. J. Cell Biol. 165, 347–356.

Hyun, D.H., Lee, M., Halliwell, B., Jenner, P., et al., 2003. Proteasomal inhibition causes the formation of protein aggregates containing a wide range of proteins, including nitrated proteins. J. Neurochem. 86, 363–373.

Ilieva, E.V., Ayala, V., Jové, M., Dalfó, E., Cacabelos, D., Povedano, M., Bellmunt, M.J., Ferrer, I., Pamplona, R., Portero-Otín, M., 2007. Oxidative and endoplasmic reticulum stress interplay in sporadic amyotrophic lateral sclerosis. Brain 130, 3111–3123.

Johnston, J.A., Dalton, M.J., Gurney, M.E., Kopito, R.R., 2000. Formation of high molecular weight complexes of mutant Cu, Zn-superoxide dismutase in a mouse model for familial amyotrophic lateral sclerosis. Proc. Natl. Acad. Sci. U. S. A. 97, 12571–12576.

Julien, J.P., 2001. Amyotrophic lateral sclerosis. Unfolding the toxicity of the misfold. Cell 104, 581–591.

Kanekura, K., Nishimoto, I., Aiso, S., Matsuoka, M., 2006. Characterization of amyotrophic lateral sclerosis-linked P56S mutation of vesicle-associated membrane protein-associated protein B (VAPB/ALS8). J. Biol. Chem. 281, 30223–30233.

Kanekura, K., Suzuki, H., Aiso, S., Matsuoka, M., 2009. ER stress and unfolded protein response in amyotrophic lateral sclerosis. Mol. Neurobiol. 39, 81–89.

Katayama, T., Imaizumi, K., Sato, N., Miyoshi, K., Kudo, T., Hitomi, J., Morihara, T., Yoneda, T., Gomi, F., Mori, Y., Nakano, Y., Takeda, J., Tsuda, T., Itoyama, Y., Murayama, O., Takashima, A., St. George-Hyslop, P., Takeda, M., Tohyama, M., 1999. Presenilim-1 mutations downregulate the signalling pathway of the unfolded protein response. Nat. Cell Biol. 1, 479–485.

Kato, S., Horiuchi, S., Liu, J., Cleveland, D.W., Shibata, N., Nakashima, K., Nagai, R., Hirano, A., Takikawa, M., Kato, M., Nakano, I., Ohama, E., 2000. Advanced glycation endproduct-modified superoxide dismutase-1 (SOD1)-positive inclusions are common to familial amyotrophic lateral sclerosis patients with SOD1 gene mutations and transgenic mice expressing human SOD1 with a G85R mutation. Acta Neuropathol. 100, 490–505.

Kikuchi, H., Almer, G., Yamashita, S., Guegan, C., Nagai, M., et al., 2006. Spinal cord endoplasmic reticulum stress associated with a microsomal accumulation of mutant superoxide dismutase-1 in an ALS model. Proc. Natl. Acad. Sci. U. S. A. 103, 6025–6030.

Kouroku, Y., Fujita, E., Jimbo, A., Kikuchi, T., Yamagata, T., Momoi, M.Y., Kominami, E., Kuida, K., Sakamaki, S., Yonehara, S., Momoi, T., 2002. Polyglutamine aggregates stimulate ER stress signal and caspase-1 activation. Hum. Mol. Genet. 11, 1505–1515.

Mackenzie, I.R., Bigio, E.H., Ince, P.G., Geser, F., Neumann, M., Cairns, N.J., Kwong, L.K., Forman, M.S., Ravits, J., Stewart, H., Eisen, A., McClusky, L., Kretzschmar, H.A., Monoranu, C.M., Highley, J.R., Kirby, J., Siddique, T., Shaw, P.J., Lee, V.M., Trojanowski, J.Q., 2007. Pathological TDP-43 distinguishes sporadic amyotrophic lateral sclerosis from amyotrophic lateral sclerosis with SOD1 mutations. Ann. Neurol. 61, 427–434.

Nakagawa, T., Zhu, H., Morishima, N., Li, E., Xu, J., Yankner, B.A., Yuan, J., 2000. Caspase-12 mediates endoplasmic reticulum-specific apoptosis and cytotoxicity by amyloid-beta. Nature 403, 98–103.

Nishimura, A.L., Mitne-Neto, M., Silva, H.C., Richieri-Costa, A., Middleton, S., Cascio, D., Kok, F., Oliveira, J.R., Gillingwater, T., Webb, J., Skehel, P., Zatz, M., 2004. A mutation in the vesicle-trafficking protein VAPB causes late-onset spinal muscular atrophy and amyotrophic lateral sclerosis. Am. J. Hum. Genet. 75, 822–831.

Okado-Matsumoto, A., Fridovich, I., 2001. Subcellular distribution of superoxide dismutases (SOD) in rat liver: Cu, Zn-SOD in mitochondria. J. Biol. Chem. 276, 38388–38393.

Rosen, D.R., Siddique, T., Patterson, D., Figlewicz, D.A., Sapp, P., et al., 1993. Mutations in Cu/Zn superoxide dismutase gene are associated with familial amyotrophic lateral sclerosis. Nature 362, 59–62.

Rowland, L.P., Schneider, N.A., 2001. Amyotrophic lateral sclerosis. N. Engl. J. Med. 344, 1688–1700.

Ryu, E.J., Harding, H.P., Angelastro, J.M., Vitolo, O.V., Ron, D., Greene, L.A., 2002. Endoplasmic reticulum stress and the unfolded protein response in cellular models of Parkinson's disease. J. Neurosci. 22, 10690–10698.

Sato, N., Imaizumi, K., Manabe, M., Taniguchi, M., Hitomi, J., Katayama, T., Yoneda, T., Morihara, T., Yasuda, Y., Takagi, T., Kudo, T., Tsuda, T., Itoyama, Y., Mukifuchi, T., Fraser, P.E., St. George-Hyslop, P., Tohyama, M., 2001. Increased production of beta-amyloid and vulnerability to endoplasmic reticulum stress by an aberrant spliced form of presenilin 2. J. Biol. Chem. 276, 2108–2114.

Schagger, H., 2006. Tricine–SDS-PAGE. Nat. Protoc. 1, 16–22.

Sturtz, L.A., Diekert, K., Jensen, L.T., Lill, R., Culotta, V.C., 2001. A fraction of yeast Cu, Zn-superoxide dismutase and its metallochaperone, CCS, localize to the intermembrane space of mitochondria. A physiological role for SOD1 in guarding against mitochondrial oxidative damage. J. Biol. Chem. 276, 38084–38089.

Tobisawa, S., Hozumi, Y., Arawaka, S., Koyama, S., Wada, M., Nagai, M., Aoki, M., Itoyama, Y., Goto, K., Kato, T., 2003. Mutant SOD1 linked to familial amyotrophic lateral sclerosis, but not wild-type SOD1, induces ER stress in COS7 cells and transgenic mice. Biochem. Biophys. Res. Commun. 303, 496–503.

Wate, R., Ito, H., Zhang, J.H., Ohnishi, S., Nakano, S., Kusaka, H., 2005. Expression of an endoplasmic reticulum-resident chaperone, glucose-regulated stress protein 78, in the spinal cord of a mouse model of amyotrophic lateral sclerosis. Acta Neuropathol. 110 (6), 557–562.

Wittig, I., Braun, H.-P., Schagger, H., 2006. Blue native PAGE. Nat. Protoc. 1, 418–428.

Wootz, H., Hansson, I., Korhonen, L., Napankangas, U., Lindholm, D., 2004. Caspase-12 cleavage and increased oxidative stress during motoneuron degeneration in transgenic mouse model of ALS. Biochem. Biophys. Res. Commun. 322, 281–286.

Yamagishi, S., Koyama, Y., Katayama, T., Taniguchi, M., Hitomi, J., Kato, M., Aoki, M., Itoyama, Y., Tohyama, N., 2007. An in vitro model for Lewy body hyaline inclusion/Astrocytic hyaline inclusion: induction by ER stress with an ALS-linked SOD1 mutation. PloS One 10, 130–140.

Yukioka, F., Matsuzaki, S., Kawamoto, K., Koyama, Y., Hitomi, J., Katayama, T., Tohyama, M., 2008. Presenilin-1 mutation activates the signaling pathway of caspase-4 in endoplasmic reticulum stress-induced apoptosis. Neurochem. Int. 52, 683–687.

# Mutations of optineurin in amyotrophic lateral sclerosis

Hirofumi Maruyama[1], Hiroyuki Morino[1], Hidefumi Ito[2]†, Yuishin Izumi[3], Hidemasa Kato[4], Yasuhito Watanabe[5],
Yoshimi Kinoshita[2], Masaki Kamada[1,3], Hiroyuki Nodera[3], Hidenori Suzuki[6], Osamu Komure[7], Shinya Matsuura[8],
Keitaro Kobatake[9], Nobutoshi Morimoto[10], Koji Abe[10], Naoki Suzuki[11], Masashi Aoki[11], Akihiro Kawata[12],
Takeshi Hirai[12], Takeo Kato[13], Kazumasa Ogasawara[14], Asao Hirano[15], Toru Takumi[5], Hirofumi Kusaka[2],
Koichi Hagiwara[16], Ryuji Kaji[3] & Hideshi Kawakami[1]

[1]Department of Epidemiology, Research Institute for Radiation Biology and Medicine, Hiroshima University, Hiroshima 734-8553, Japan.
[2]Department of Neurology, Kansai Medical University, Moriguchi 570-8506, Japan. [3]Department of Clinical Neuroscience, University of
Tokushima Graduate School, Tokushima 770-8503, Japan. [4]Division of Developmental Biology, Research Center for Genomic Medicine,
Saitama Medical University, Saitama 350-1241, Japan. [5]Laboratory of Integrative Bioscience, Hiroshima University Graduate School of
Biomedical Sciences, Hiroshima 734-8553, Japan. [6]Faculty of Human Science, Hiroshima Bunkyo Women's University, Hiroshima 731-
0295, Japan. [7]South Osaka Neurosurgical Hospital, Osakasayama 589-0011, Japan. [8]Department of Genetics and Cell Biology, Research
Institute for Radiation Biology and Medicine, Hiroshima University, Hiroshima 734-8553, Japan. [9]Department of Neurology, Kobatake
Hospital, Fukuyama 720-1142, Japan. [10]Department of Neurology, Okayama University, Graduate School of Medicine, Dentistry, and
Pharmaceutical Sciences, Okayama 700-8558, Japan. [11]Department of Neurology, Tohoku University School of Medicine, Sendai 980-8574,
Japan. [12]Department of Neurology, Tokyo Metropolitan Neurological Hospital, Fuchu, Tokyo 183-0042, Japan. [13]Department of Neurology,
Haematology, Metabolism, Endocrinology and Diabetology, Yamagata University Faculty of Medicine, Yamagata 990-9585, Japan.
[14]Department of Pathology, School of Medicine, Shiga University of Medical Science, Ohtsu 520-2192, Japan. [15]Division of Neuropathology,
Department of Pathology, Montefiore Medical Center, New York, New York 10467-2490, USA. [16]Department of Respiratory Medicine,
Saitama Medical University, Saitama 350-0495, Japan. †Present address: Department of Neurology, Kyoto University Graduate School of
Medicine, Kyoto 606-8507, Japan.

# Mutations of optineurin in amyotrophic lateral sclerosis

Hirofumi Maruyama[1], Hiroyuki Morino[1], Hidefumi Ito[2]†, Yuishin Izumi[3], Hidemasa Kato[4], Yasuhito Watanabe[5], Yoshimi Kinoshita[2], Masaki Kamada[1,3], Hiroyuki Nodera[3], Hidenori Suzuki[6], Osamu Komure[7], Shinya Matsuura[8], Keitaro Kobatake[9], Nobutoshi Morimoto[10], Koji Abe[10], Naoki Suzuki[11], Masashi Aoki[11], Akihiro Kawata[12], Takeshi Hirai[12], Takeo Kato[13], Kazumasa Ogasawara[14], Asao Hirano[15], Toru Takumi[5], Hirofumi Kusaka[2], Koichi Hagiwara[16], Ryuji Kaji[3] & Hideshi Kawakami[1]

Amyotrophic lateral sclerosis (ALS) has its onset in middle age and is a progressive disorder characterized by degeneration of motor neurons of the primary motor cortex, brainstem and spinal cord[1]. Most cases of ALS are sporadic, but about 10% are familial. Genes known to cause classic familial ALS (FALS) are superoxide dismutase 1 ($SOD1$)[2], $ANG$ encoding angiogenin[3], $TARDP$ encoding transactive response (TAR) DNA-binding protein TDP-43 (ref. 4) and fused in sarcoma/translated in liposarcoma ($FUS$, also known as $TLS$)[5,6]. However, these genetic defects occur in only about 20–30% of cases of FALS, and most genes causing FALS are unknown. Here we show that there are mutations in the gene encoding optineurin ($OPTN$), earlier reported to be a causative gene of primary open-angle glaucoma (POAG)[7], in patients with ALS. We found three types of mutation of $OPTN$: a homozygous deletion of exon 5, a homozygous Q398X nonsense mutation and a heterozygous E478G missense mutation within its ubiquitin-binding domain. Analysis of cell transfection showed that the nonsense and missense mutations of $OPTN$ abolished the inhibition of activation of nuclear factor kappa B (NF-κB), and the E478G mutation revealed a cytoplasmic distribution different from that of the wild type or a POAG mutation. A case with the E478G mutation showed OPTN-immunoreactive cytoplasmic inclusions. Furthermore, TDP-43- or SOD1-positive inclusions of sporadic and $SOD1$ cases of ALS were also noticeably immunolabelled by anti-OPTN antibodies. Our findings strongly suggest that OPTN is involved in the pathogenesis of ALS. They also indicate that NF-κB inhibitors could be used to treat ALS and that transgenic mice bearing various mutations of $OPTN$ will be relevant in developing new drugs for this disorder.

We analysed six Japanese individuals from consanguineous marriages who had ALS; two of them were siblings, the others were from independent families. We used homozygosity mapping, which has been shown to identify a locus of a disease-causing gene from as few as three individuals[8]. We performed a genome-wide scan of single nucleotide polymorphisms (SNPs) by using the GeneChip Human Mapping 500K Array Set (Affymetrix), and selected for the run of homozygous SNPs (RHSs) more than 3 centimorgans in length. Under this condition, the RHSs are able to retrieve more than 98%

of the entire length of the autozygous segments created as a result of a first-cousin or second-cousin marriage (Supplementary Information)[8]. We extracted RHSs of six individuals (Supplementary Fig. 1a). A region (hg18: 12,644,480–15,110,539) in chromosome 10, which was an overlap among four subjects, was chosen as the primary candidate region (Supplementary Fig. 1b). Assuming that subjects ii, iii, v and vi had the same disease gene, the chance that the overlap had the disease gene was $P_{ii+iii+v+vi} = 0.935$ (Supplementary Information). We listed up to 17 candidate genes in the region and sequenced their exons (Supplementary Fig. 1c). We detected a deletion of exon 5 in the $OPTN$ (also known as FIP-2 (ref. 9)) gene in two siblings (Fig. 1a, family 1, subjects 1 and 2). PCR with a forward primer of exon 4 and a reverse primer of intron 5 revealed a 2.5-kilobase (kb) band in the control, V-3 and IV-1, and a 0.7-kb band in IV-1, subject 1 and subject 2 (Fig. 1b). Direct sequence analysis of the short band showed the joining of the 5′ part of AluJb in intron 4 and the 3′ part of AluSx in intron 5 with 12-base-pair (bp) microhomology (Fig. 1c). Thus, the deletion resulted from Alu-mediated recombination. We also found a homozygous nonsense c.1502C>T mutation (Q398X, exon 12) in the gene in one individual with ALS (Fig. 1d, e, family 2, subject 3). For the other three subjects, we found neither mutations nor copy number changes in the $OPTN$ gene, although we did not completely exclude the possibility of mutations in introns or intergenic regions in the gene. We extended our analysis of $OPTN$ to ten additional individuals from consanguineous marriages who had ALS, 76 individuals with familial ALS and 597 individuals with sporadic ALS (SALS). We found the Q398X mutation in a sporadic individual (subject 4, family 3; Fig. 1d). Subjects 3 and 4, who were not related according to their family history, shared their haplotype for a 0.9-megabase (Mb) region (hg18: chr10: 12,973,261–13,879,735) containing the $OPTN$ gene (Supplementary Table 1). We investigated a total of 170 copies of chromosome 10 from 85 Japanese subjects genotyped for the HapMap3 project, and found that the incidental length of haplotype sharing around $OPTN$ gene was at most 320 kb. Given that a haplotype sharing of 0.9 Mb rarely occurs by chance, the mutation is likely to have been derived from a single ancestor (Supplementary Fig. 1d). Subjects 1 and 2 shared their haplotype for an 8.3-Mb

[1]Department of Epidemiology, Research Institute for Radiation Biology and Medicine, Hiroshima University, Hiroshima 734-8553, Japan. [2]Department of Neurology, Kansai Medical University, Moriguchi 570-8506, Japan. [3]Department of Clinical Neuroscience, University of Tokushima Graduate School, Tokushima 770-8503, Japan. [4]Division of Developmental Biology, Research Center for Genomic Medicine, Saitama Medical University, Saitama 350-1241, Japan. [5]Laboratory of Integrative Bioscience, Hiroshima University Graduate School of Biomedical Sciences, Hiroshima 734-8553, Japan. [6]Faculty of Human Science, Hiroshima Bunkyo Women's University, Hiroshima 731-0295, Japan. [7]South Osaka Neurosurgical Hospital, Osakasayama 589-0011, Japan. [8]Department of Genetics and Cell Biology, Research Institute for Radiation Biology and Medicine, Hiroshima University, Hiroshima 734-8553, Japan. [9]Department of Neurology, Kobatake Hospital, Fukuyama 720-1142, Japan. [10]Department of Neurology, Okayama University, Graduate School of Medicine, Dentistry, and Pharmaceutical Sciences, Okayama 700-8558, Japan. [11]Department of Neurology, Tohoku University School of Medicine, Sendai 980-8574, Japan. [12]Department of Neurology, Tokyo Metropolitan Neurological Hospital, Fuchu, Tokyo 183-0042, Japan. [13]Department of Neurology, Haematology, Metabolism, Endocrinology and Diabetology, Yamagata University Faculty of Medicine, Yamagata 990-9585, Japan. [14]Department of Pathology, School of Medicine, Shiga University of Medical Science, Ohtsu 520-2192, Japan. [15]Division of Neuropathology, Department of Pathology, Montefiore Medical Center, New York, New York 10467-2490, USA. [16]Department of Respiratory Medicine, Saitama Medical University, Saitama 350-0495, Japan. †Present address: Department of Neurology, Kyoto University Graduate School of Medicine, Kyoto 606-8507, Japan.
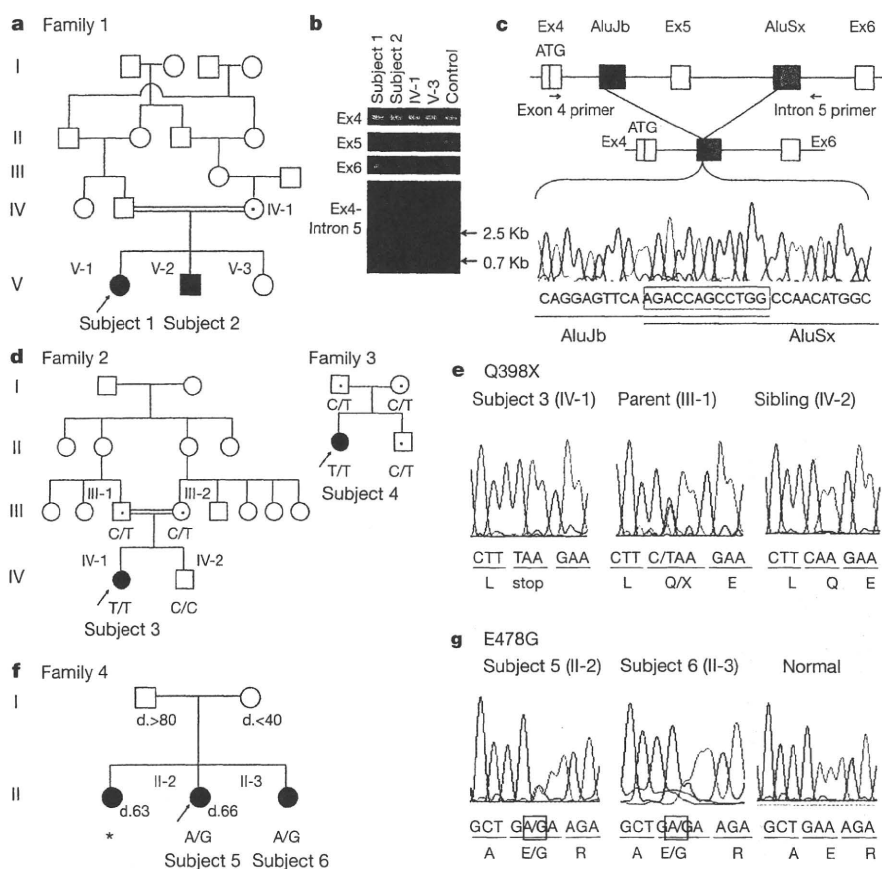
**Figure 1 | Exon 5 deletion, nonsense and missense mutations of the *OPTN* gene. a,** Family 1. The filled circle or square indicate the affected individuals; the arrows indicate the probands. **b,** Agarose gel electrophoretogram. Subject 1 (V-1) and subject 2 (V-2) showed lack of exon 5 PCR product and shortened product of exon 4 to intron 5. **c,** Chromatogram with OPTN deletion of exon 5 and schematic structure of deleted gene. **d,** Families 2 and 3. Dots indicate heterozygous carriers. **e,** Chromatograms from index subjects with OPTN mutation of c.1502 C>T. Homozygous mutation is in red, and the mutation is indicated by using the single-letter amino-acid code. **f,** Family 4. *DNA sample could not be obtained. Numerals show the age at death. **g,** Chromatograms from index subjects with the OPTN mutation of c.1743A>G. The heterozygous mutation is marked by the square.

region (hg18: chr10: 6,815,934–14,842,351), which contained the *OPTN* gene and was different from that in subjects 3 and 4 (Supplementary Table 1).

In the screening of ALS families, we identified a heterozygous missense mutation (c1743A>G, E478G, exon14, Fig. 1g) of *OPTN* in four individuals with ALS in two families with ALS. Subjects 5 and 6 were sisters, and the pedigree suggests that the mutation had an autosomal dominant trait with incomplete penetrance (Fig. 1f, family 4). Subjects 7 and 8 (family 5) were brothers. Although these families are not related according to their family history, subjects 5–8 shared their haplotype for 2.3 Mb (hg18: chr10: 11,460,985–13,703,017, Supplementary Table 3), again suggesting that the mutation was derived from a single ancestor. Indeed, the Q398X nonsense and E478G missense mutations were not observed in 781 healthy Japanese volunteers as well as in over 6,800 (including 1,728 Japanese) individuals in the glaucoma studies, where the entire coding region of the gene was investigated (Supplementary Table 2). Collectively, the mutation was absent over a total of 5,000 Japanese chromosomes. The deletion mutation was also absent in 200 Japanese, and not reported in the over 6,800 glaucoma individuals. The co-segregation of three different mutations of *OPTN* with the ALS phenotype strongly suggests that some mutations of *OPTN* cause ALS.

The eight individuals with mutations of *OPTN* showed onset from 30 to 60 years of age. Most of them showed a relatively slow progression and long duration before respiratory failure, although the clinical phenotypes were not homogeneous (see Supplementary Information).

The Q398X mutation causes a premature stop during translation, truncating the 577 amino-acid OPTN protein to one of 397 amino acids in length. This truncation results in a deletion of the coiled coil 2 domain[10], which is necessary for binding to ubiquitin[11], huntingtin[12] (htt), myosin VI[13] and the ubiquitinated receptor-interacting protein[14]. In the gene with the deletion of exon 5, if there was a transcript,

the transcript splicing from exon 4 to exon 6 would cause a frame shift and make a stop codon (TGA in the ninth to eleventh codons in exon 6), which would be expected to translate a peptide 58 amino acids in length. The missense mutation (E478G) was located between coiled coil 2 domain and the leucine zipper domain. This glutamic acid is highly conserved among OPTN proteins of a wide range of species (Supplementary Fig. 2a), and is situated within the DFxxER motif, an ubiquitin-binding domain shared among OPTN, NF-κB essential molecule (NEMO), and A20 binding and inhibitor of NF-κB proteins (ABIN) (Supplementary Fig. 2b). The mutations in the DFxxER motif in ABIN reduce the binding to ubiquitin, which render them unable to inhibit NF-κB activation[11]. We investigated the ability of various mutations of *OPTN* to inhibit NF-κB-mediated transcriptional activation by performing a luciferase assay using NSC-34 cells (a mouse neuroblastoma and spinal-cord hybrid cell line) transfected with wild-type or mutant *OPTN*. E50K *OPTN*, which causes POAG[7], downregulated the NF-κB activity, as did the wild type. On the other hand, both Q398X and E478G had no ability to inhibit NF-κB activity (Tukey–Kramer, $P < 0.05$). These tendencies were retained after stimulation with tumour-necrosis factor (TNF)-α (Fig. 2A). We also examined the subcellular localization of overexpressed Flag-tagged wild-type OPTN (wild type) and its mutants in cells (Fig. 2B). Immunofluorescence staining was performed with their antibodies against Flag and the Golgi matrix marker GM130. Confocal images showed close apposition of granular signals of wild-type OPTN or E50K with GM130 (see g and i in Fig. 2B)[15,16]. E50K often shapes large granular structures near the Golgi apparatus. E478G rarely showed granular signals (see b in Fig. 2B); however, when closely observed, some of the signals were still closely localized to GM130 (see h in Fig. 2B). Western blotting using a lysate of transformed lymphoblasts showed that the 74-kDa band, corresponding to OPTN, was absent in subjects 3 and 4, but was present in the non-diseased mother and brother of subject 3 (Supplementary Fig. 3a). Quantitative PCR with reverse transcription
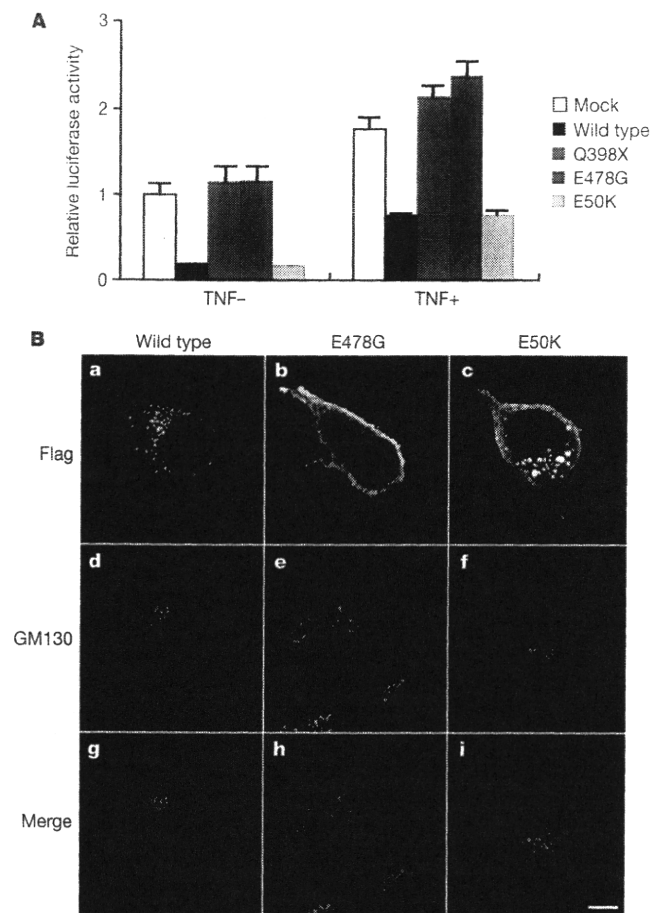
**Figure 2 | Influence of OPTN mutations. A,** Luciferase assay to assess the ability of various OPTNs to inhibit activation of NF-κB. The wild type and E50K have a similar NF-κB activation-inhibiting effect, whereas mock, Q398X and E478G types lack this effect. Error bars, standard deviations of triplicate assays. **B,** Localization of OPTN. Flag is the white signals in a–c and red signals in g–i. GM130 is the white signals in d–f and green signals in g–i. The wild type shows many fluorescent granules closely localized with the Golgi apparatus. E478G OPTN shows a reduced number of granules, and rarely co-localized with the Golgi apparatus. E50K OPTN granules have become large and closely localized with the Golgi apparatus. Scale bar, 10 μm.

revealed that the products were diminished to 58.0% in the hetero-zygote (III-2) and to 13.8% in the homozygote (subject 4) compared with the control levels (Supplementary Fig. 3b). In addition, cyclo-heximide recovered the decrease in the OPTN messenger RNA (mRNA) with the mutation (Supplementary Fig. 3c). Thus mRNA with this mutation, which bears a premature termination, might be degraded through nonsense-mediated mRNA decay in lymphoblasts.

The spinal cord from subject 5 with the E478G mutation revealed loss of myelin from the corticospinal tract and of the anterior horn cells (AHCs, Fig. 3a and Supplementary Fig. 4a, b). OPTN immuno-histochemistry demonstrated increased staining intensity of the cytoplasm of the remaining AHCs and the neurites in the anterior horn (Supplementary Fig. 4c). Higher magnification of the motor neurons revealed intracytoplasmic eosinophilic inclusions (Fig. 3b, d). Intriguingly, these inclusions were distinctly immunopositive for OPTN (Fig. 3c, e). On the other hand, the cytoplasm of AHCs from control individuals was faintly labelled with anti-OPTN antibodies (Supplementary Fig. 5a, c), similar to the spinal-cord AHCs of mice (Supplementary Fig. 6b) and in contrast to the highly labelled sensory neurons in the dorsal root ganglia of mice (Supplementary Fig. 6d). In patients with sporadic ALS, the staining intensity for OPTN apparently increased not only in the cytoplasm of the remaining AHCs but also in their neurites (Supplementary Fig. 5b, d). In
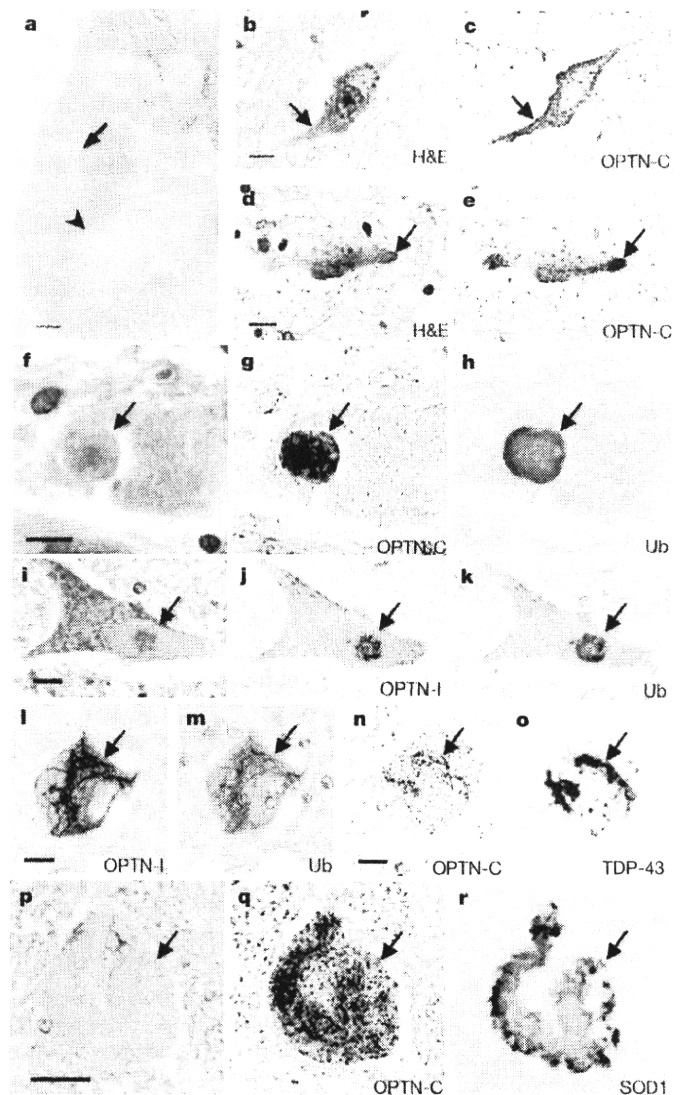


**Figure 3 | Identification of OPTN in distinctive intracytoplasmic inclusions of subjects with ALS. a–e,** Neuropathology of the lumbar spinal cord from subject 5. Klüver-Barrera (**a**) show loss of myelin from the corticospinal tract (arrow) and loss of motor neurons from the anterior horn (arrowhead). The cytoplasm of the remaining motor neurons contains an amorphous eosinophilic region (**b**, arrow). H&E, haematoxylin and eosin. The same neuron was re-stained with the anti-OPTN antibody (**c**, arrow). The eosinophilic retention occasionally appears to form a hyaline inclusion (**d**, arrow), which is intensely immunolabelled with the anti-OPTN antibody (**e**, arrow). **f–k,** Round hyaline inclusions of subjects with SALS (**f**, **i**) are immunolabelled with anti-OPTN-C and anti-OPTN-I antibodies (**g** and **j**, respectively). The sections were re-stained with anti-ubiquitin (Ub) antibodies (**h**, **k**). **l–o,** Skein-like inclusions of patients with SALS are reactive with the anti-OPTN-I and anti-OPTN-C antibodies (**l**, **n**). Re-staining of **l** with the anti-ubiquitin antibody (**m**) and **n** with anti-TDP-43 antibody (**o**). **p–r,** Lewy-body-like hyaline inclusion of a patient with FALS, stained with haematoxylin and eosin (**p**), anti-OPTN-C antibody (**q**) and SOD1 antibody (**r**). Scale bars, 200 μm (**a**), 20 μm (**b–p**).

addition, distinctive intracytoplasmic inclusions were also noticeably OPTN immunolabelled in cases of sporadic and familial ALS; eosinophilic round hyaline inclusions from patients with SALS were immunopositive for OPTN (Fig. 3f, g, i, j). Re-staining of the same sections for ubiquitin, a known constituent of many neuro-degenerative inclusions, revealed that these inclusions were also positive and faithfully matched the distribution of OPTN immuno-reactivity (Fig. 3h, k). The anti-OPTN antibodies also stained skein-like inclusions (Fig. 3l, n), which were again mirrored with the anti-ubiquitin antibodies (Fig. 3m) and with the anti-TDP-43

antibodies (Fig. 3o). The distinct OPTN immunoreactivity of ubiquitin- and TDP-43-positive intracytoplasmic inclusions was confirmed on serial sections from patients with SALS (Supplementary Fig. 7). Moreover, SOD1-immunopositive Lewy-body-like hyaline inclusions from cases with *SOD1* FALS were also immunopositive for OPTN (Fig. 3p–r). We found that OPTN antibody labelled both SOD1- and TDP-43-positive inclusions. As the staining of SOD1 and TDP-43 is generally mutually exclusive, OPTN staining appears to be a more general marker for inclusions in various types of ALS; therefore, the OPTN molecule might also be involved in a broader pathogenesis of ALS.

The mutations of the *OPTN* gene cause both recessive and dominant traits, and the mechanism causing the disease may be different between the two traits. The Q398X nonsense mutation and probably the exon 5 deletion mutation cause a decrease in OPTN expression resulting from nonsense-mediated mRNA decay of the transcript carrying the nonsense OPTN mutations. Therefore, the mutated OPTN protein by itself is unlikely to disturb cell function or to be included in the inclusion body in the motor neuron cells. The mechanism of recessive mutations causing ALS is expected to be simply loss of function, and the heterozygote for the Q398X mutation does not develop the ALS phenotype. On the other hand, the E478G missense mutation increased the immunoreactivity for OPTN in the cell body and the neurites. The increased amount and different distribution of the mutated protein would disturb neuronal functions, and may accelerate the inclusion body formation as well as the increase and the different distribution of OPTN immunoreactivity in sporadic ALS. Thus the heterozygote for the E478G mutation will develop the disease.

The different impact on NF-κB signalling and the different intracellular localization of ALS- and POAG-linked mutated protein may explain the phenotypic divergence between the two diseases. Subject 3 with homozygotic Q398X also showed POAG, whereas subject 4 with the same mutation, and subjects 1 and 2 with the exon 5 deletion, did not show it. The prevalence of POAG in the population older than 40 years is 3.9% in Japan[17].Considering this information, the ALS and glaucoma in subject 3 may accidentally coexist.

OPTN competes with NEMO for binding to the ubiquitinated receptor-interacting protein and negatively regulates TNF-α-induced activation of NF-κB[14], which mediates an upregulation of OPTN, creating a negative feedback loop[18]. ALS-related OPTN mutations lacked the inhibitory effect towards NEMO, and thus exaggerated NF-κB activation. In sporadic ALS, a previous report showed that NF-κB, which is classified as a 'cell death inhibitor', is upregulated in motor neurons[19]. The upregulated NF-κB may induce the overexpression of OPTN, and may also cause neuronal cell death[20]. Thus NF-κB is a major candidate target for treating this disease. Additionally OPTN plays an important role in the maintenance of the Golgi complex, in membrane trafficking, in exocytosis, through its interaction with myosin VI and Rab8 (ref. 13), and in post-Golgi trafficking to lysosomes dependent on the Rab8/OPTN/htt complex[21] (Supplementary Fig. 8). Interestingly, FUS/TLS has been reported to interact with myosin VI[22] as well as with myosin V[23]. Impairment of intracellular trafficking of the complex including OPTN and/or FUS/TLS may cause inclusions in this neurodegenerative disorder.

## METHODS SUMMARY

**Genotyping and extraction of candidate regions.** The genotype of the GeneChip Human Mapping 500K Array Set (Affymetrix) was performed by AROS Applied Biotechnology. Computer analyses of the SNPs were performed by a homozygosity mapping algorithm accommodated to the whole-genome SNP scan data (Supplementary Information). To investigate the existence of a large insertion or deletion in this region, we analysed the copy number using Affymetrix Genotyping Console version 4.0 for the Affymetrix Mapping 500K data.

1. Leigh, P. N. in *Handbook of Clinical Neurology: Amyotrophic Lateral Sclerosis* Vol. 82 (eds Eisen, A. A. & Shaw, P. J.) 249–278 (Elsevier, 2007).
2. Rosen, D. R. *et al.* Mutations in Cu/Zn superoxide dismutase gene are associated with familial amyotrophic lateral sclerosis. *Nature* 362, 59–62 (1993).
3. Greenway, M. J. *et al. ANG* mutations segregate with familial and 'sporadic' amyotrophic lateral sclerosis. *Nature Genet.* 38, 411–413 (2006).
4. Sreedharan, J. *et al.* TDP-43 mutations in familial and sporadic amyotrophic lateral sclerosis. *Science* 319, 1668–1672 (2008).
5. Kwiatkowski, T. J. *et al.* Mutations in the *FUS/TLS* gene on chromosome 16 cause familial amyotrophic lateral sclerosis. *Science* 323, 1205–1208 (2009).
6. Vance, C. *et al.* Mutations in FUS, an RNA processing protein, cause familial amyotrophic lateral sclerosis type 6. *Science* 323, 1208–1211 (2009).
7. Rezaie, T. *et al.* Adult-onset primary open-angle glaucoma caused by mutations in optineurin. *Science* 295, 1077–1079 (2002).
8. Huqun, et a. I. Mutations in the SLC34A2 gene are associated with pulmonary alveolar microlithiasis. *Am. J. Respir. Crit. Care Med.* 175, 263–268 (2007).
9. Li, Y., Kang, J. & Horwitz, M. S. Interaction of an adenovirus E3 14.7-kilodalton protein with a novel tumor necrosis factor alpha-inducible cellular protein containing leucine zipper domains. *Mol. Cell. Biol.* 18, 1601–1610 (1998).
10. Schwamborn, K., Weil, R., Courtois, G., Whiteside, S. T. & Iaraël, A. Phorbol esters and cytokines regulate the expression of the NEMO-related protein, a molecule involved in a NF-κB-independent pathway. *J. Biol. Chem.* 275, 22780–22789 (2000).
11. Wagner, S. *et al.* Ubiquitin binding mediates the NF-κB inhibitory potential of ABIN proteins. *Oncogene* 27, 3739–3745 (2008).
12. Hattula, K. & Peränen, J. FIP-2, a coiled-coil protein, links hutingtin to Rab8 and modulates cellular morphogenesis. *Curr. Biol.* 10, 1603–1606 (2000).
13. Sahlender, D. A. *et al.* Optineurin links myosin VI to the Golgi complex and is involved in Golgi organization and exocytosis. *J. Cell Biol.* 169, 285–295 (2005).
14. Zhu, G., Wu, C. J. & Ashwell, J. D. Optineurin negatively regulates TNFα-induced NF-κB activation by competing with NEMO for ubiquitinated RIP. *Curr. Biol.* 17, 1438–1443 (2007).
15. De Marco, N., Buono, M., Troise, F. & Diez-Roux, G. Optineurin increases cell survival and translocates to the nucleus in a Rab8-dependent manner upon an apoptotic stimulus. *J. Biol. Chem.* 281, 16147–16156 (2006).
16. Chalasani, M. L., Balasubramanian, D. & Swarup, G. Focus on molecules: optineurin. *Exp. Eye Res.* 87, 1–2 (2008).
17. Iwase, A. *et al.* The prevalence of primary open-angle glaucoma in Japanese: the Tajimi Study. *Ophthalmology* 111, 1641–1648 (2004).
18. Mrowka, R., Blüthgen, N. & Fähling, M. Seed-based systematic discovery of specific transcription factor target genes. *FEBS J.* 275, 3178–3192 (2008).
19. Jiang, Y. M. *et al.* Gene expression profile of spinal motor neurons in sporadic amyotrophic lateral sclerosis. *Ann. Neurol.* 57, 236–251 (2005).
20. Pizzi, M. & Spano, P. Distinct roles of diverse nuclear factor-κB complexes in neuropathological mechanisms. *Eur. J. Pharmacol.* 545, 22–28 (2006).
21. Toro, D. *et al.* Mutant huntingtin impairs post-Golgi trafficking to lysosomes by delocalizing optineurin/Rab8 complex from the Golgi apparatus. *Mol. Biol. Cell* 20, 1478–1492 (2009).
22. Takarada, T. *et al.* A protein–protein interaction of stress-responsive myosin VI endowed to inhibit neural progenitor self-replication with RNA binding protein, TLS, in murine hippocampus. *J. Neurochem.* 110, 1457–1468 (2009).
23. Yoshimura, A. *et al.* Myosin-Va facilitates the accumulation of mRNA/protein complex in dendritic spines. *Curr. Biol.* 16, 2345–2351 (2006).

**Author Contributions** H. Kawakami designed and supervised the study. H.Mo. and K.H. extracted candidate genes. H.Ma. and M.K. performed sequencing analysis. H.Ma., H.Mo., Y.W., T.T., S.M., H. Kawakami and H.S. conducted molecular biological analysis. H.I., Y.K., H. Ku., H. Kato, K.O. and A.H. performed pathological analysis and provided pathological samples. Y.I., H.N., R.K., O.K., N.M., K.A., A.K., T.H, T.K., M.A., N.S. and K.K. collected clinical information and samples. H. Kawakami, H.Ma., H.I. and K.H. wrote the paper.

**Author Information** Reprints and permissions information is available at www.nature.com/reprints. The authors declare no competing financial interests. Correspondence and requests for materials should be addressed to H. Kawakami (hkawakam@hiroshima-u.ac.jp).
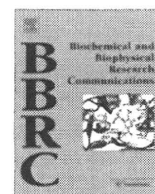
# Segmental copy-number gain within the region of isopentenyl diphosphate isomerase genes in sporadic amyotrophic lateral sclerosis

Takeo Kato [a,*,1], Mitsuru Emi [a,b,1], Hidenori Sato [a,b,1], Shigeki Arawaka [a], Manabu Wada [a], Toru Kawanami [a], Tadashi Katagiri [c], Kenji Tsuburaya [d], Itaru Toyoshima [e], Fumiaki Tanaka [f], Gen Sobue [f], Kenichi Matsubara [b]

[a] Department of Neurology, Haematology, Metabolism, Endocrinology, and Diabetology, Yamagata University Faculty of Medicine, Yamagata, Japan
[b] CNV Laboratory, DNA Chip Research Institute, Yokohama, Japan
[c] Yamagata Prefectural Kahoku Hospital, Yamagata, Japan
[d] NHO Yamagata National Hospital, Yamagata, Japan
[e] Department of Medical Education, Akita University School of Medicine, Akita, Japan
[f] Department of Neurology, Nagoya University School of Medicine, Nagoya, Japan

## ARTICLE INFO

## ABSTRACT

Aims: Sporadic amyotrophic lateral sclerosis (SALS) seems to be a multifactorial disease, the pathogenesis of which may involve both genetic and environmental factors. The present study aims at identifying a possible genetic change that confers risk for SALS. Methods: We performed whole-genome screening of a copy-number variation (CNV) using a CNV beadchip, followed by real-time quantitative polymerase chain reaction (qPCR) and region-targeted high-density oligonucleotide tiling microarray. Results: Within the 40-kb region on 10p15.3 subtelomere, which harbours two genes encoding isopentenyl diphosphate isomerase 1 (IDI1) and IDI2, we found a segmental copy-number gain in a large proportion of SALS patients. qPCR analysis demonstrated the copy-number gain in 46 out of 83 SALS patients, as compared with 10 out of 99 controls ($p = 4.86 \times 10^{-11}$, Odds Ratio 10.8); subsequent tiling microarray validated qPCR results and elucidated the fine structure of segmental gains. Conclusions: A segmental copy-number gain in the IDI1/IDI2 gene region may play a significant role in the pathogenesis of SALS.

© 2010 Elsevier Inc. All rights reserved.

## 1. Introduction

Amyotrophic lateral sclerosis (ALS) is a fatal neurodegenerative disease characterised by the degeneration of motor neurons. ALS has two forms: familial ALS (FALS) and sporadic ALS (SALS). FALS is a rare, monogenic disease for which several causal genes have been identified [1], including the optineurin gene, which we found recently [2].

SALS comprises the majority (90–98%) of ALS cases. Although the aetiology of SALS remains unknown, the results of a British motor neuron disease twin study suggested the importance of a genetic component in SALS [3]. Genome-wide association studies using single-nucleotide polymorphisms (SNPs) have been attempted, and some studies found significant associations of some SNPs with SALS [4–8]. However, other studies did not disclose such findings after correction for multiple testing [9–11]. Moreover, the

SNPs reported to be significantly associated with SALS were not necessarily replicated in the studies published thereafter [11,12].

Recently, copy-number variations (CNVs), such as the deletion or gain (duplication, triplication, etc.) of a genomic region, have been recognised as inter-individual genetic variations [13]. Indeed, several CNV abnormalities are significant in the aetiology of sporadic and inherited diseases (reviewed in [14]).

In order to identify a possible genetic change that confers a risk for SALS, we conducted a whole-genome CNV analysis. Here, we report a segmental copy-number gain within the region harbouring the isopentenyl diphosphate isomerase (IDI) genes on 10p15.3 subtelomere in many patients with SALS.

## 2. Materials and methods

### 2.1. Subjects

The present study included 83 patients with SALS who fulfilled the criteria for probable or definite ALS according to the 1994 El Escorial criteria [15]. One hundred control subjects were randomly selected from among community-dwelling elderly individuals with no neurological diseases [16,17]. There were no significant differences in mean age (SALS/control = 59.9/70.0 years) or ratio of

* Corresponding author. Address: Department of Neurology, Haematology, Metabolism, Endocrinology, and Diabetology, Yamagata University Faculty of Medicine, 2-2-2 Iida-Nishi, Yamagata 990-9585, Japan. Fax: +81 23 628 5318.
E-mail address: tkato@med.id.yamagata-u.ac.jp (T. Kato).
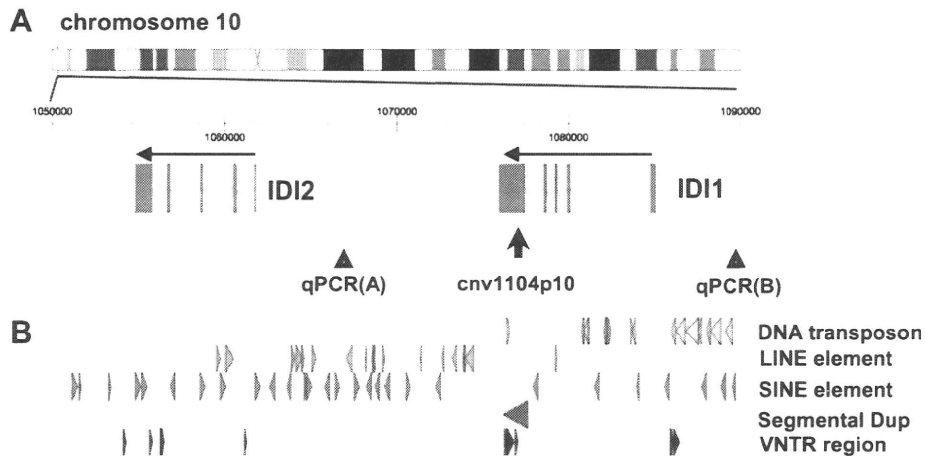[1] These authors contributed equally to this work.

**Fig. 1.** Localisation of IDI1 and IDI2 genes on 10p15.3 subtelomere region. (A) The vertical arrow and arrowheads indicate the positions of the CNV marker (cnv1104p10) and qPCR primers, respectively. Top panel shows ideogram of chromosome 10 and the positions of IDI1 and IDI2 genes. (B) Multiple complex repetitive structures in the region of IDI1 and IDI2 genes: DNA transposon; LINE element; SINE element; segmental Dup; and VNTR region.

men to women (SALS/control = 1.27/0.76) between the two groups ($p$ = 0.38 and 0.1, respectively). DNA was extracted from peripheral blood leukocytes. All participants gave written informed consent for genetic analysis. The study was approved by the Medical Ethics Committee of Yamagata University Faculty of Medicine.

### 2.2. Screening with whole-genome CNV beadchip

We conducted whole-genome screening by using the deCODE-Illumina CNV beadchip (57K, i-select format, Illumina Infinium system, deCODE genetics, Inc., Iceland). The platform was designed with CNV probes to target CNV-rich regions of the whole genome, such as megasatellites (tandem repeats > 500 bp), duplicons (region flanked by highly homologous segmental duplication > 1 kb), unSNPable region (>15 kb gaps in HapMap SNP map, and, 5–15 kb gaps with >2SNPs with Hardy–Weinberg failure), and CNVs registered in Database of Genomic Variants. It contained 15,559 CNV segments, covering 190 Mb, or 6% of the human genome; these segments were 18-fold enriched as compared with average human genome. CNV data were analysed by Dosage Miner program as described previously [18].

### 2.3. TaqMan quantitative PCR (qPCR)

DNA samples were assayed for copy number of the region of IDI1 gene (Fig. 1A) on 10p15.3 using Applied Biosystems TaqMan Gene Copy Number Assays in triplicates (qPCR) as instructed by the manufacturer. Primers and probes were designed from genomic sequence (hg18/Build 36) using Applied Biosystems proprietary software. Each assay was run as a triplex TaqMan real-time PCR, using an FAM dye-based assay targeted to 10p region and a VIC dye-based assay for the reference gene, RNase P (PN 4316844 from Applied Biosystems). Each PCR assay was performed in triplicate. Data analysis was performed as described previously [19].

### 2.4. High-density oligonucleotide tiling microarray analysis

Agilent's high-density oligonucleotide tiling microarray assay was performed on a custom-designed microarray, which targeted to the 40-kb subtelomeric region harbouring the IDI1/IDI2 genes on 10p15.3 (Chr10: 1,050,000–1,090,000 [NCBI Build 36.1, hg18]) as described previously [20]. Detection of abnormal copy number,
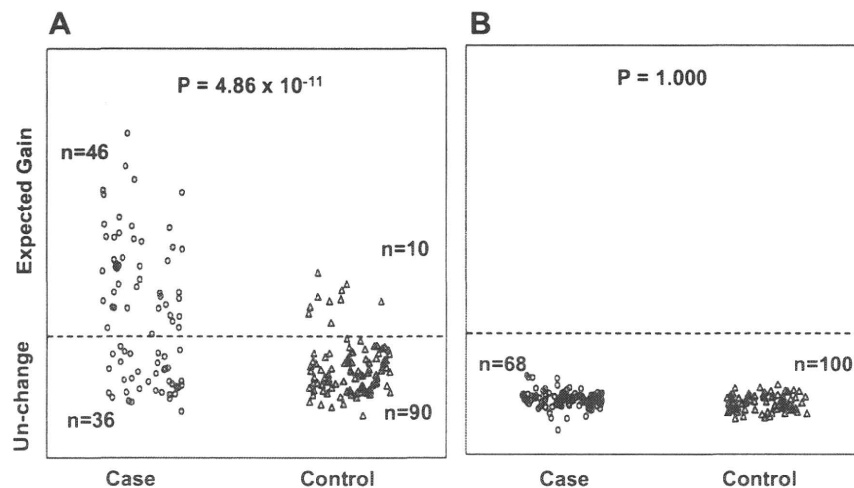


**Fig. 2.** qPCR analysis for copy-number change. (A) Gain was detected by qPCR analysis within the IDI1/IDI2 gene region in a large proportion of SALS patients (left plots), as compared with controls (right plots). (B) No such difference in copy number is observed outside the region between the two groups. The locations of the qPCR primer sets for (A) and (B) are shown in Fig. 1A.